Basin Research

IAS EAGE

Basin Research (2012) **24**, 1–27, doi: 10.1111/j.1365-2117.2012.00547.x

Miocene sedimentation, volcanism and deformation in the Eastern Cordillera (24°30′ S, NW Argentina): tracking the evolution of the foreland basin of the Central Andes

Luigina Vezzoli,[1] Valerio Acocella,[2] Ricardo Omarini[3] and Roberto Mazzuoli[4]

[1]*Dipartimento di Scienza e Alta Tecnologia, Universita' dell'Insubria, Como, Italy*
[2]*Dipartimento di Scienze Geologiche, Universita' di Roma Tre, Rome, Italy*
[3]*Facultad de Ciencias Naturales, Universidad Nacional de Salta, Salta, Argentina*
[4]*Dipartimento di Scienze della Terra, Universita' degli Studi di Pisa, Pisa, Italy*

ABSTRACT

Understanding the relationships between sedimentation, tectonics and magmatism is crucial to defining the evolution of orogens and convergent plate boundaries. Here, we consider the lithostratigraphy, clastic provenance, syndepositional deformation and volcanism of the Almagro-El Toro basin of NW Argentina (24°30′ S, 65°50′ W), which experienced eruptive and depositional episodes between 14.3 and 6.4 Ma. Our aims were to elucidate the spatial and temporal record of the onset and style of the shortening and exhumation of the Eastern Cordillera in the frame of the Miocene evolution of the Central Andes foreland basin. The volcano-sedimentary sequence of the Almagro-El Toro basin consists of lower red floodplain sandstones and siltstones, medial non-volcanogenic conglomerates with localised volcanic centres and upper volcanogenic coarse conglomerates and breccia. Coarse, gravity flow-dominated (debris-flow and sheet-flow) alluvial fan systems developed proximal to the source area in the upper and medial sequence. Growing frontal and intrabasinal structures suggest that the Almagro-El Toro portion of the foreland basin accumulated on top of the eastward-propagating active thrust front of the Eastern Cordillera. Synorogenic deposits indicate that the shortening of the foreland deposits was occurring by 11.1 Ma, but conglomerates derived from the erosion of western sources suggest that the uplift and erosion of this portion of the Eastern Cordillera has occurred since *ca.*12.5 Ma. An unroofing reconstruction suggests that 6.5 km of rocks were exhumed. A tectono-sedimentary model of an episodically evolving thick-skinned foreland basin is proposed. In this frame, the NW-trending, transtensive Calama–Olacapato–El Toro (COT) structures interacted with the orogen, influencing the deposition and deformation of synorogenic conglomerates, the location of volcanic centres and the differential tilt and exhumation of the foreland.

INTRODUCTION

Knowledge of the synorogenic sedimentation and structure of foreland basin systems provide key information about the location, timing and kinematics of major deformation events within mountain belts (e.g. Beck *et al.*, 1988; DeCelles *et al.*, 1991, 1998; Hendrix *et al.*, 1992; Horton & DeCelles, 1997). In this regard, Tertiary sedimentary rocks from the Eastern Cordillera of the Central Andes may provide diagnostic information regarding depositional environments, mechanisms of synorogenic deformation and timing of sediment-source exhumation during the Andean mountain building (Allmendinger *et al.*, 1983; Jordan & Alonso, 1987; Isacks, 1988; Horton, 1998; Strecker *et al.*, 2009).

The Central Andes at 24–26° S coincides with the boundary between tectonomorphic provinces of the Eastern Cordillera, Santa Barbara System, Sierras Pampeanas and Puna plateau (Fig. 1), as well as major transverse features, such as the Calama–Olacapato–El Toro (COT) fault zone (Allmendinger *et al.*, 1983; Riller *et al.*, 2001; Matteini *et al.*, 2002; Acocella *et al.*, 2011), accompanied by back-arc magmatism (Riller *et al.*, 2001; Mazzuoli *et al.*, 2008; Gioncada *et al.*, 2010; Petrinovic *et al.*, 2010).

Studies addressing the Tertiary foreland differentiation of the Central Andes focused on the Bolivian Eastern Cordillera, N of 24° S (e.g. Kley *et al.*, 1997; Horton,

Correspondence: L. Vezzoli, Dipartimento di Scienza e Alta Tecnologia, Universita' dell'Insubria, via Valleggio 11, 22100 Como, Italy. E-mail: luigina.vezzoli@uninsubria.it

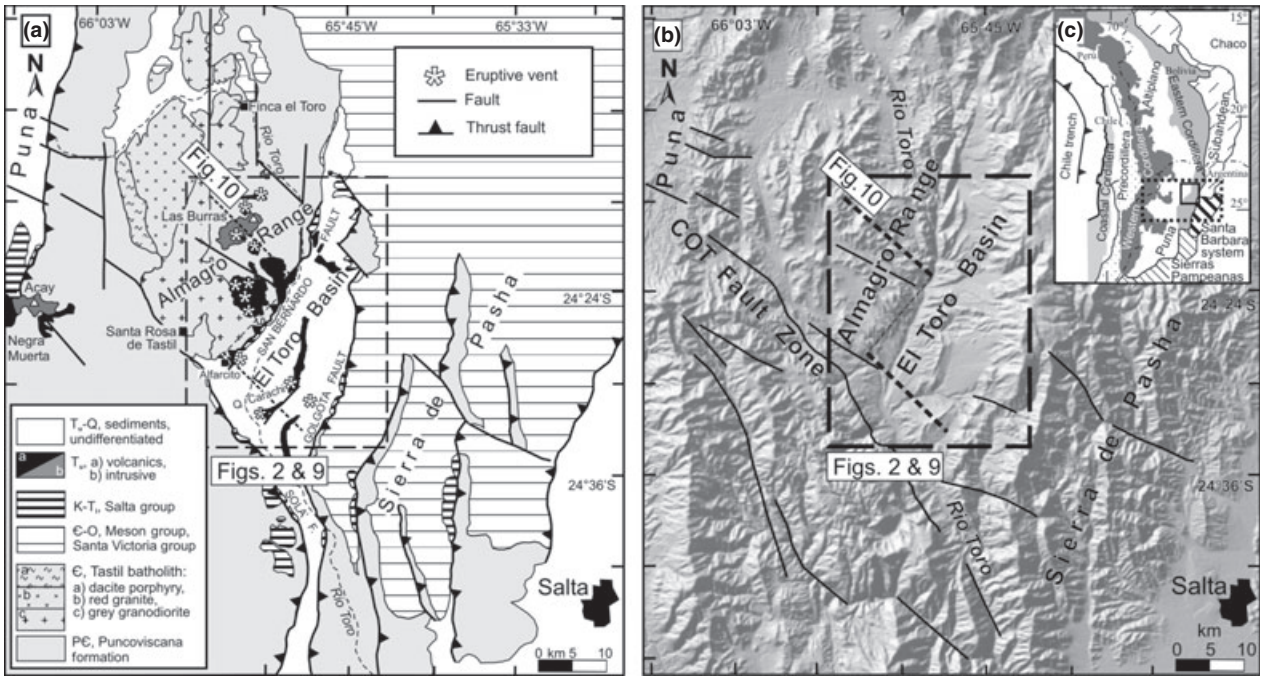

Fig. 1. Geologic map (a) and digital elevation model (b) of the Eastern Cordillera at *ca.* 24°30′ S (NW Argentina). The distribution of pre-Miocene rocks depicts the main sources of non-volcanic clasts in the Cenozoic El Toro basin fill. The box indicates the area mapped in Figs 2 and 9; the hashed line indicates the transect shown in Fig. 10. (c) Regional geologic setting of Central Andes. The black box shows the location of study area; dotted box is the area mapped in Fig. 11a.

1998, 2005; Coutand *et al.*, 2001; Siks & Horton, 2011), the Eastern Cordillera, S of 25° S (e.g. Strecker *et al.*, 1989; Bossi *et al.*, 2001; Starck & Anzótegui, 2001; Kley & Monaldi, 2002; Coutand *et al.*, 2006; Deeken *et al.*, 2006; Carrera & Muñoz, 2008; Hain *et al.*, 2011) and the Sierras Pampeanas, S of 26° S (e.g. Davila & Astini, 2007; Mortimer *et al.*, 2007; Iaffa *et al.*, 2011).

The different deformation styles of the Andean foreland are attributed mainly to the distinct configurations of the subducting Nazca plate (Barazangi & Isacks, 1976; Jordan *et al.*, 1983). However, regional studies suggest that the inherited paleogeographic and structural pre-Andean features controlled the along-strike segmentation of the foreland (Allmendinger *et al.*, 1983; Kley *et al.*, 1999) as suggested by the following: (a) the uplift and southward exposure of progressively deeper levels of the Proterozoic–lower Paleozoic basement prior to the Cretaceous (Allmendinger *et al.*, 1983); (b) the different thickness and distribution of Paleozoic rocks (Turner, 1970; Sanchez & Salfity, 1999) and (c) the structural segmentation of the Cretaceous Salta rift basin (Marquillas & Salfity, 1988; Grier *et al.*, 1991; Fig. 1).

Within the Eastern Cordillera, the non-marine basin of the quebrada de El Toro (Fig. 1; Marrett *et al.*, 1994; Marrett & Strecker, 2000; Hilley & Strecker, 2005) was part of a continuous foreland basin before 6.4 Ma (Viramonte *et al.*, 1994; Reynolds *et al.*, 2000; Hilley & Strecker, 2005; Mazzuoli *et al.*, 2008; Hain *et al.*, 2011; also this study); Pliocene–Pleistocene contraction and uplift fragmented it into basins and ranges (Strecker *et al.*, 1989; Marrett *et al.*, 1994; Kleinert & Strecker, 2001).

This field-based study combines stratigraphical, sedimentological, structural, geochronological and volcanological data along a transect crossing the basement-involved Almagro range and the contiguous intermontane El Toro basin at 24°30′ S and 65°50′ W, within the Eastern Cordillera of NW Argentina (Fig. 1). The non-marine sedimentary deposits (Schwab & Schäfer, 1976; Marrett & Strecker, 2000; Hilley & Strecker, 2005) are interlayered with the products of the middle-upper Miocene Las Burras–Almagro-El Toro (BAT) magmatic complex (Mazzuoli *et al.*, 2008). These dated volcanic horizons furnish chronologic constraints on synorogenic depositional and tectonic processes, which are not present in the Eastern Cordillera immediately to the N and S. Component analysis of synorogenic conglomerates constrains provenance rock types and the timing of unroofing of the exhumed and uplifted source areas (e.g. Graham *et al.*, 1986; DeCelles *et al.*, 1991, 1993; Horton *et al.*, 2002).

The first purpose of this study was to document the synorogenic relationships between sedimentation, volcanism and deformation in the Almagro-El Toro area during the middle-late Miocene. The second purpose was to use these data to improve reconstructions of the spatial and temporal evolution of the Eastern Cordillera. Finally, we discuss some key points relevant to a general tectono-sedimentary model for thick-skinned foreland basins.

Our results describe the development of the Andean foreland basin system at the eastern margin of the Puna plateau during the middle-late Miocene. This period coincides with the onset of the Neogene deformation and

with the incorporation of this part of the foreland system into the thick-skinned fold-thrust belt, as orogenic deformation of the frontal ranges propagated eastward.

GEOLOGICAL AND STRUCTURAL SETTING

The Eastern Cordillera developed E of the Puna plateau (Fig. 1c) and consists of N-trending, basement-involved folds bounded by bivergent thrust and back-thrust faults, at times with a strike-slip component, with intervening Tertiary sedimentary basins (Fig. 1; Kley *et al.*, 1996; Hilley & Strecker, 2005; Acocella *et al.*, 2007). Deformation and uplift of the southern Eastern Cordillera probably started in Eocene (Hongn *et al.*, 2007; Payrola Bosio *et al.*, 2009). Major shortening of the Eastern Cordillera started at 20–15 Ma (Allmendinger *et al.*, 1997; Jordan *et al.*, 1997) and developed during the middle Miocene (Jordan & Alonso, 1987; Hernandéz *et al.*, 1999; Reynolds *et al.*, 2000). This shortening produced nearly exclusive thrust faulting parallel to the border of the Puna plateau and accommodated E–W to NW–SE horizontal shortening. A Pliocene–Quaternary oblique-slip regime with N–S extension was related to NE–SW and E–W shortening (Marrett *et al.*, 1994; Marrett & Strecker, 2000).

At *ca.* 24°30′ S, the NW-striking COT lineament is a zone of major sinistral strike-slip faulting (Marrett *et al.*, 1994; Acocella *et al.*, 2011) focusing back-arc magmatic centres (Riller *et al.*, 2001; Matteini *et al.*, 2002; Petrinovic *et al.*, 2005; Fig. 1). This magmatism, distributed over >300 km E of the active arc (Western Cordillera; Fig. 1c), occurred from 17 Ma (Petrinovic *et al.*, 2010) to the Quaternary (Coira *et al.*, 1993). The main volcanic activity developed between 11 and 6 Ma (Acocella *et al.*, 2011). The BAT complex, ranging in age from 14.3 to 6.4 Ma (Mazzuoli *et al.*, 2008), is the easternmost back-arc magmatism along the COT fault zone (Figs 1 and 2).

The stratigraphic features at *ca.* 24°30′ S suggest a thickness of *ca.* 6.5 km for the potential source of the

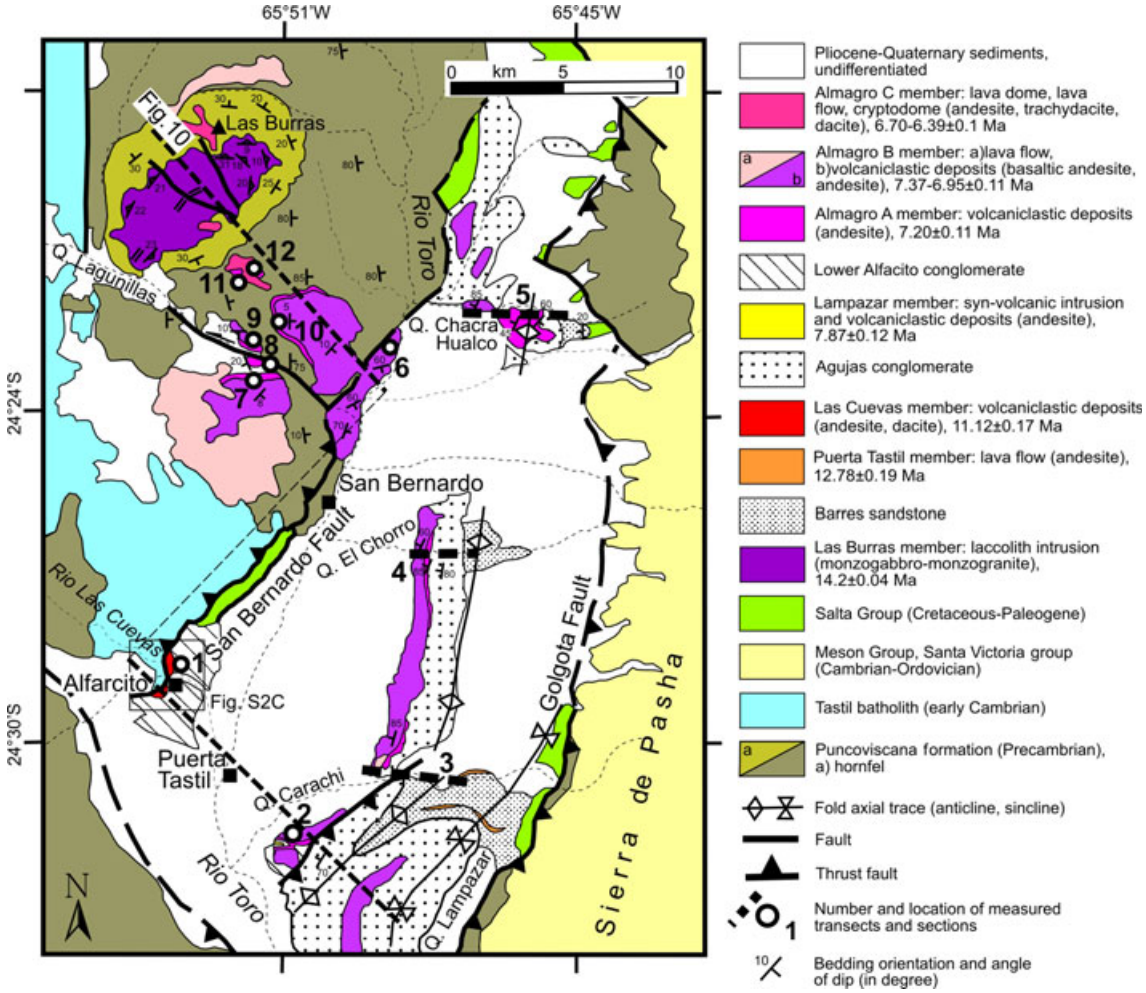

Fig. 2. Geologic map of the Almagro range and El Toro basin, based on our original field mapping (see Fig. 1 for location). The stratigraphy of the synorogenic sequence of the El Toro basin is temporally constrained by dated members of the BAT magmatic complex (Mazzuoli *et al.*, 2008). The numbers indicate the location of measured sections and transects through Cenozoic strata discussed in the text. The hashed line indicates the transect shown in Fig. 10. The box is Fig. S2C.

foreland deposits. The basement is represented largely by the Neoproterozoic-Lower Cambrian low-grade metasedimentary sequence of the Puncoviscana Formation (Figs 1 and 2), consisting of dark grey and purple quarzitic sandstone, siltstone and shale, and which is >2000 m thick (Mon, 1999; Omarini *et al.*, 1999). Regionally, lower Paleozoic marine strata unconformably overlie the metasedimentary basement (Fig. 1). The Lower-Middle Cambrian Meson Group, *ca.* 160 m thick (fig. 4 in Sanchez & Salfity, 1999), includes stratified, fine-grained, whitish and pink quartzite with intercalation of greenish shale beds (Turner, 1970; Sanchez & Salfity, 1999). The Upper Cambrian-Lower Ordovician Santa Victoria Group has a maximum thickness of *ca.* 2300 m and comprises fine- to medium-grained greenish sandstone alternating with shale and quarzitic sandstone (Turner, 1970; Moya, 1999). The upper Neoproterozoic-Cambrian Tastil batholith consists of grey granodiorite, red granite and dacite porphyry (Fig. 1) intruding the Neoproterozoic-lower Paleozoic sequence (Kilmurray & Igarzabal, 1971; Hongn *et al.*, 2010).

The Cretaceous-Paleogene Salta Group (Marquillas & Salfity, 1988; Marquillas *et al.*, 2005) represents a rift basin system unconformably overlying Paleozoic rocks or the Puncoviscana Formation (Fig. 1). Its thickness is highly variable; in our study area, the postrift sequence (late Campanian-middle Eocene) has an estimated thickness of $\geq$2000 m (figs 4 and 5 in Marquillas & Salfity, 1988). This sequence is represented by shallow marine, oolitic and stromatolitic, yellowish limestone and marl (Balbuena Subgroup, Yacoraite Formation) and non-marine red sandstone and mudstone (Santa Barbara Subgroup).

The study area lies within the Eastern Cordillera at *ca.* 24°30′ S and 65°50′ W, approximately 40 km E of the Puna plateau margin, and comprises the uplifted basement block of the Almagro range (at an average elevation of 3800 m above sea level; a.s.l.) and the intermontane El Toro basin (at *ca.* 3000 m a.s.l.; Figs 1 and 2).

The N-trending Almagro basement block extends for *ca.* 70 km along strike and exhibits a 3.5-km-thick rock sequence plunging to the NE (Fig. 1). Exposures of the upper Neoproterozoic-Cambrian Tastil batholith are limited to the Almagro range (Fig. 1).

The El Toro basin is N-S elongated, funnel-shaped in map view (60 km long, 1–20 km wide) and bounded by two oppositely verging high-angle reverse faults (Figs 1 and 2). A 50-km-long, N-trending anticline in the medial El Toro basin forms a prominent ridge (Figs 2 and S1A).

Along the W side of the El Toro basin, the W-dipping San Bernardo Fault (Marrett *et al.*, 1994) places basement rocks of the Almagro range on Cretaceous-Cenozoic strata. The E-dipping Golgota Fault (Marrett *et al.*, 1994), which probably became active after the deposition of the middle-upper Miocene volcano-sedimentary rocks (Hilley & Strecker, 2005; Mazzuoli *et al.*, 2008), defines the E basin margin. The Sierra de Pasha forms the hangingwall of the Golgota Fault and exposes an unroofed stratigraphic section >1700 m thick, comprising the Neoproterozoic-Paleogene sequence, with the Puncoviscana Formation forming a broad thrust-related frontal anticline (Acocella *et al.*, 2007) and the Salta Group strata capping the lower Paleozoic section (Figs 1 and 2). Salta Group strata are also involved in thrust sheets and overturned synclines in the footwall of the San Bernardo, Golgota and Sola' Faults (Marrett *et al.*, 1994; Marrett & Strecker, 2000; Acocella *et al.*, 2007; Figs 1 and 2). SW of the El Toro basin, the lower Paleozoic section was eroded prior to the sedimentation of the Cretaceous-Paleogene Salta Group strata (Fig. 1). The westernmost outcrop of this unit in the study area consists of a NNE-trending, folded range NE of the Nevado de Acay (Fig. 1; Blasco *et al.*, 1996).

MATERIALS AND METHODS

The lithostratigraphy of volcanic and sedimentary units was based on lithofacies, composition, petro-chemistry and cross-cutting and overlapping relationships. The stratigraphic reconstruction includes the correlation of volcanic and sedimentary sequences between the Almagro range and El Toro basin (Fig. 2). The compositional characteristics of the volcanic rocks support the correlation of the volcanic deposits in proximal and distal areas. Previously published Rb/Sr and K/Ar dates (Mazzuoli *et al.*, 2008) provide the chronostratigraphic framework for the studied deposits.

Twelve stratigraphic transects across Miocene strata were measured (Fig. 2). On the El Toro basin, the volcano-sedimentary sequence is exposed along E-trending stream gorges (quebradas) perpendicular to the strike of the strata. Along each transect, the sequence was reconstructed with metre resolution. Sections representative of major depositional systems were measured with decimetre resolution to characterize sedimentation styles and stratigraphic contacts.

Sedimentary facies were defined and interpreted using lithology, grain size and depositional structures (Table 1; Miall, 1978; Smith & Lowe, 1991). Volcanic facies and terminology for nonexplosive fragmental volcanic materials were used as defined by McPhie *et al.* (1993). Primary volcanic facies have been described and interpreted by Mazzuoli *et al.* (2008) and Vezzoli *et al.* (2009). Identification and counts of conglomerate clasts were conducted on conglomerate and breccia beds. Conglomerate compositions were determined on the field by counting at least 100 clasts >2.5 cm in apparent size using square-metre grids and by image analysis on calibrated digital photographs. Few measurements of paleocurrent directions were taken on rare imbricated clasts in gravel beds, correcting any tilting and folding of the strata.

The orogenic deformations were defined through field analysis of slip data on fault planes (Acocella *et al.*, 2007, 2011; Mazzuoli *et al.*, 2008), unconformities and growth

Table 1. Summary of sedimentary lithofacies and interpretation used in this study

Facies code*	Facies type	Units†	Sedimentary characteristics	Interpretation
Resedimented syneruptive facies				
RBmm	Matrix-supported, massive, volcanogenic breccia	LC	Stratified, very coarse breccia, poorly sorted, disorganised; primary volcanic clast textures unmodified; jigsaw-fit texture; average clast size 5–30 cm; maximum size 1.5–2 m; sandy to granular, vitric matrix	Chilling and brecciation of lava in water; subaerial or subaqueous volcanic debris flows
RBcm/mm	Clast- to matrix-supported, massive, volcanogenic breccia	AB	Coarse breccia, poorly sorted, normal, inverse and inverse-normal grading; roughly stratified in massive beds; angular to sub-angular clasts; crystal-rich, sandy to granular matrix	Autoclastic fragmentation of lava flows; volcanic debris avalanches, debris flows, and hyperconcentrated flows
RGcm	Clast-supported, massive, volcanogenic conglomerate	AA	Pebble-boulder conglomerate, moderately to poorly sorted, vitric sandy matrix; locally normal graded, imbricated and with a channel-like erosional base	Autoclastic fragmentation of lava domes; recycled? non-volcanic clasts; channelised debris flows or shallow traction currents by high-competency water flow
Volcanogenic sedimentary facies				
VGcm	Clast-supported, massive, volcanogenic conglomerate	LC, LP, AA	Pebble-boulder conglomerate, locally matrix-supported, moderately to well sorted, disorganised to imbricated; sandy to granular matrix; well-rounded clasts, outsized clasts >90 cm	Pyroclastic, autoclastic and epiclastic fragmentation; recycled? non-volcanic clasts; subaerial or subaqueous debris flows and hyperconcentrated flows
VGmm/cm	Matrix- to clast-supported, massive, volcanogenic conglomerate	AA, AB	Pebble-boulder conglomerate, disorganised or imbricated, erosional basal surface and crude upward-fining texture; subangular to subrounded volcanic clasts, outsized clasts > 100–300 cm; crystal- and lithic-rich sandy matrix	Epiclastic fragmentation; recycled? non-volcanic clasts; unconfined debris-avalanche and debris flows transitional to hyperconcentrated flows
VSm	Massive, volcanogenic sandstone	AA, AB	Medium to fine sandstone, structureless or faintly laminated	Suspension-settling in flood-plain lakes and ponds, scour fills
VSh	Stratified volcanogenic sandstone	LP, AA, AB	Fine to coarse sandstone and pebbly sandstone, moderately to well sorted, planar- and low-angle (<15°) cross-laminated	Stream flows and scour fills
TFml	Tuffaceous siltstone and mudstone (tuffite)	AgC	Vitric, planar-laminated, white fine siltstone to mudstone	Pyroclastic fragmentation; suspension-settling in pond or lake
Non-volcanogenic sedimentary facies				
Gmm	Matrix-supported, massive conglomerate	AgC	Cobble-pebble conglomerate, poorly sorted, unstratified, disorganized; subangular to subrounded clasts, 0.5–20 cm in diameter; locally clast-supported, outsized boulder clasts (>50 cm), faintly horizontal stratification, reverse grading; coarse-grained sandy matrix; tabular and non-erosive	Sheet-like, non-cohesive debris flows transitional to hyperconcentrated flows

(continued)

Table 1 (continued)

Facies code*	Facies type	Units†	Sedimentary characteristics	Interpretation
Gmm/cm	Matrix-to clast-supported, massive conglomerate	LAC	Cobble–pebble conglomerate, moderately to poorly sorted, disorganised; sheet-like beds, 0.5–3.0 m thick, extends laterally for tens to hundreds of metres; angular to subrounded clasts, maximum size 10–25 cm; sandy matrix; planar non-erosional base	Laminar, sandy debris flow in dispersed alluvial fans
Gcm	Clast-supported, massive conglomerate	BS, LAC	Granule-boulder conglomerate, moderately to poorly sorted, disorganised or poorly organised, locally imbricated; subrounded clasts; sandy matrix; lenticular channel-like beds, erosional base	Poorly confined channel filling during higher discharge or channelised non-cohesive debris flows
Gch	Clast- to matrix-supported, crudely bedded conglomerate	LAC	Granule-cobble conglomerate, moderately sorted, upward fining; horizontally stratified, partly amalgamated beds; angular to subangular clasts; sandy matrix; erosional base at decimetre scale	Hyperconcentrated sheet floods and high-density turbulent flows in dispersed alluvial fans
Bcm	Clast-supported, massive breccia	AA	Monogenetic breccia, angular to subangular clasts; open texture or granule to coarse sandy matrix	Debris talus
Sm	Massive sandstone	BS, AgC	Fine- to medium-grained sandstone, structureless or faintly laminated, in tabular non-erosional beds a few cm to dm thick	Sandy debris flows or sheet-flows or dilute waning stage of hyperconcentrated flows.
Sm/h	Massive or stratified, graded sandstone	LAC	Fine to coarse sandstone and siltstone, normal graded; non-erosional base	Hyperconcentrated flows and moderate sediment concentration water flows.
Sh	Horizontally stratified sandstone	BS	Fine- to medium-grained sandstone and sandy siltstone, moderately to well sorted, planar-laminated, in tabular non-erosional beds a few centimetre to decimetre thick	Sheet-floods, overbank flows or waning-stage channels
Fsl	Laminated siltstone (mudstone)	BS	Red, green or grey siltstone, planar-laminated	Sheet-floods or suspension-settling in ponds and lakes
Fsm	Massive siltstone (mudstone)	AgC	Yellow or reddish siltstone, disorganised or faintly laminated	Waning-flow conditions
P	Paleosol	AgC	Massive, mottled, reddish siltstone and mudstone, chemical weathered pebbles, clay nodules, polygonal structures	Pedogenetic alteration

*Lithofacies codes modified after Miall (1978) and DeCelles *et al.* (1991, 2007)).
†Lithostratigraphic units code: AA, Almagro A member; AB, Almagro B member; AC, Almagro C member; AgC, Agujas conglomerate; BS, Barres sandstone; LP, Lampazar member; LA, Las Cuevas member; LAC, Lower Alfarcito conglomerate.

strata, and detailed mapping of geometric and relative age relationships between structures and basin fill. The timing of fault movements and folding has been directly dated based on synsedimentary structures.

STRATIGRAPHY AND FACIES ANALYSIS

The rocks of the study area in the Central Andean foreland basin system consist of andesite and dacite lavas and

breccias of the BAT magmatic complex (Mazzuoli *et al.*, 2008; Vezzoli *et al.*, 2009) and the non-marine clastic fill of the El Toro basin (Schwab & Schäfer, 1976; Marrett & Strecker, 2000; Hilley & Strecker, 2005).

The products of the BAT magmatic complex have been subdivided into seven genetically distinct lithostratigraphic members (Fig. 2) defined by Mazzuoli *et al.* (2008). Abrupt chemical changes in the magma composition allow the division of the BAT activity into two phases.

The older magmatic phase (14.3–12.8 Ma) comprises the Las Burras monzogabbro-monzogranite (Las Burras member) and the oldest volcanic unit (Puerta Tastil member). The Las Burras member is dated at 14.3 Ma (Mazzuoli *et al.*, 2008) and consists of a NE-elongated laccolith, *ca.* 3.5 × 7 km wide, showing a NE-trending feeder in its southern part. It intruded the Puncoviscana Formation (Fig. 2). Considering the estimated thickness of the Precambrian–Mesozoic rock column (Turner, 1970; Marquillas & Salfity, 1988; Mon, 1999) and the Las Burras laccolith thickness, the probable depth of the intrusion was *ca.* 6.5 km. The intrusion presently reaches 4150 m a.s.l. in the Almagro range. Lavas of the youngest volcanic unit, the Almagro C member (dated at 6.39 ± 0.10 Ma; Mazzuoli *et al.*, 2008), unconformably cap the unroofed top of the Las Burras laccolith.

The younger magmatic phase (11.1–6.4 Ma) comprises five volcanic units. In order of decreasing age, they are Las Cuevas, Lampazar, Almagro A, Almagro B and Almagro C members (Fig. 2; Mazzuoli *et al.*, 2008). Andesite and dacite lavas were extruded from monogenetic vents in the form of flows and domes; they are associated and genetically related to extensive, coarse volcaniclastic deposits. Pyroclastic rocks are scanty. Lithofacies of the Las Cuevas, Lampazar and Almagro A members show evidence of magma–water interaction (Vezzoli *et al.*, 2009).

In the Almagro range, the BAT volcanic units rest on a basal angular unconformity representing a polycyclic erosion surface cut into the Neoproterozoic-Cambrian metamorphic and intrusive basement rocks. Eastward, BAT volcanic members are widely interbedded on the non-marine clastic sedimentary succession of the El Toro basin (Fig. 2; Mazzuoli *et al.*, 2008). All contacts between volcanic and sedimentary units are sharp, strengthened by textural and lithologic differences, erosional and/or unconformable surfaces and lack of grading.

The sedimentary sequence of the El Toro basin is >2000 m thick (Hilley & Strecker, 2005). The geometry and chronology of the contact between the Salta Group (Paleocene–middle Eocene Santa Barbara Subgroup) and Neogene strata are poorly accessible and documented. For the El Toro sedimentary units, we adopt the stratigraphic nomenclature proposed by Marrett & Strecker (2000) and Hilley & Strecker (2005), where the basin fill comprises three sets of Neogene sedimentary units, each separated by unconformity (Fig. 2). The sedimentation of the oldest set (Barres sandstone and Agujas conglomerate) ends at *ca.* 8 Ma. The intermediate set (lower Alfarcito, Solà and upper Alfarcito conglomerates) includes an extrabasinal tephra layer of 4.17 Ma (Marrett & Strecker, 2000). The upper set (Carachi conglomerate) comprises an extrabasinal tephra layer of 0.98 Ma (Marrett *et al.*, 1994). The Neogene sequence is deformed and eroded to form a paleotopographic surface prior to the sedimentation of the late Pleistocene–Holocene El Mollar conglomerate (Trauth & Strecker, 1999). The previously described Pliocene–Holocene strata of the El Toro basin (Hilley & Strecker, 2005) are not included in this study. Rather, we focused on the Miocene sedimentary sequence coeval with the BAT magmatic activity. Our data on the stratigraphic relations between volcanic and sedimentary units allow us to define accurately the stratigraphy and areal extent of the Agujas and lower Alfarcito conglomerates and to suggest a correlation between the lower Alfarcito and Solá conglomerates.

The following paragraphs describe key lithofacies and discuss the depositional systems (Table 1) of the sedimentary (Barres sandstone, Agujas conglomerate and lower Alfarcito conglomerate) and volcanic (Puerta Tastil, Las Cuevas, Lampazar, Almagro A, B and C members) interbedded units, in order of decreasing age.

Barres sandstone

The Barres sandstone (Figs 2 and S1A) is *ca.* 350 m thick and composed dominantly of grey and reddish, non-volcanogenic, planar-laminated sandstone interbedded with mudstone, siltstone and massive sandstone facies (Sh, Fsl and Sm; Table 1). The subordinate, granule-cobble conglomerate facies (Gcm; Table 1) occurs as lenticular or discontinuous layers a few metres wide.

Interpretation

Barres sandstone possibly represents a sand-dominated distal alluvial fan or floodplain system deposited by predominant, unconfined sheetflow (Sh, Fsl and Sm) with occasional, poorly confined, broad channels that were filled during higher discharge (Gcm) (Hubert & Hyde, 1982; Hampton & Horton, 2007, and references therein).

Puerta Tastil member

The coherent lava facies of Puerta Tastil member consists of plagioclase-phyric andesite (K/Ar age of 12.78 ± 0.19 Ma; Mazzuoli *et al.*, 2008) forming irregular tabular bodies intercalated into and concordant with the Barres sandstone and extending laterally for several tens and hundreds of metres (Figs 2 and S1).

Interpretation

The coherent plagioclase-phyric andesite represents lava flows extruded from vents probably located near the current exposures in the quebrada Carachi.

Agujas conglomerate

The Agujas conglomerate (Sections 3, 4 and 5; Figs 2 and 3) consists of a > 700-m-thick sequence of roughly stratified, non-volcanogenic conglomerate facies (Gmm), grading upward into massive or weakly bedded sandstone (Sm) and siltstone (Fsm) facies (Table 1; Fig. 4). Atop and within this unit, reddish, clay-rich paleosols (P; Table 1) were recognised (Figs 3 and 4)

Interpretation

Conglomerate beds (Gmm) of the Agujas conglomerate result from non-cohesive debris flows transitional to hyperconcentrated flows (Blair & McPherson, 1994). The upward grading into sandy deposits (Sm and Fsm) may reflect deposition from the dilute waning stage of the hyperconcentrated flows (Pierson & Costa, 1987). The laterally extensive, sheet-like geometry of the conglomerate and finer beds without erosive scours and channels suggest the depositional environment of the proximal–medial area of an alluvial fan system dominated by laterally unconfined, sediment-rich flows. An intraformational, planar-laminated, white tuffaceous fine siltstone facies (TFml; Table 1 and Fig. 3c) is interpreted as an extrabasinal tephra layer, probably resedimented in a pond or lake (tuffite).

Las Cuevas member

The Las Cuevas member (Section 1; Figs 2, 8 and S2) is 11.12 ± 0.17 Ma (Mazzuoli *et al.*, 2008), *ca.* 70 m thick and includes five primary volcanic facies (Vezzoli *et al.*, 2009), one resedimented syneruptive breccia facies (RBmm) and one volcanogenic sedimentary conglomerate facies (VGcm) (Table 1; Fig. 5).

Interpretation

The resedimented syneruptive breccia facies (RBmm) represents deposition from sediment gravity flows, with negligible clast modification during transport, caused by the failure of quenched, subaqueous margins of lava domes (Vezzoli *et al.*, 2009). The volcanogenic sedimentary conglomerate facies (VGcm) is interpreted as a mixture of clasts derived from autoclastic, pyroclastic and

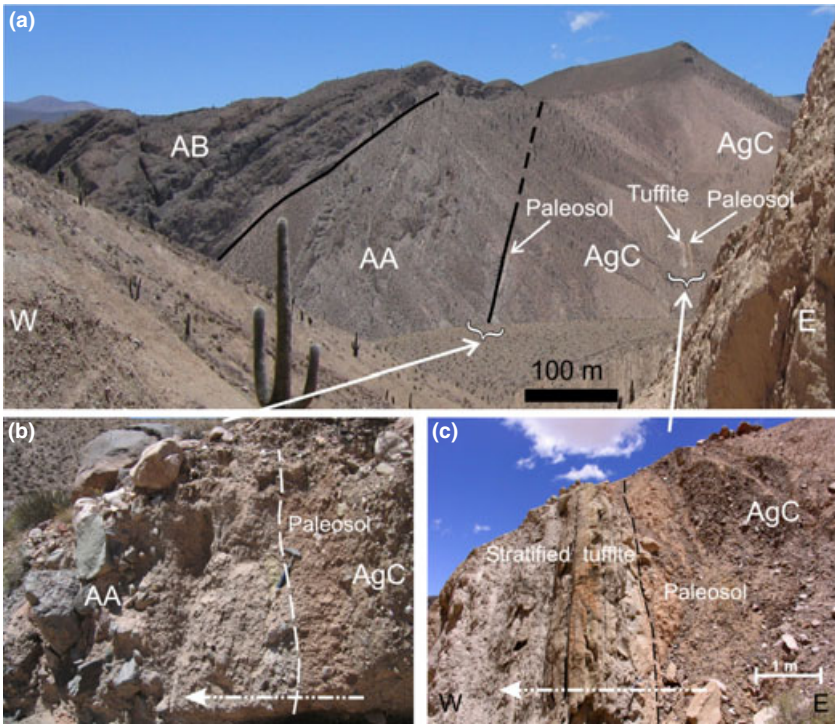

Fig. 3. The stratigraphic transect along the quebrada El Chorro (Section 4 in Fig. 2). (a) Overview of the W limb of the intrabasinal anticline deforming the Neogene El Toro basin strata. The stratigraphic sequence becomes younger westward. A paleosol outlines the paraconcordant contact between the Almagro A member (AA) and Agujas conglomerate (Fig. 3b). The paleosol and tuffite beds couple encased within the Agujas conglomerate (AgC) is magnified in Fig. 3c. The basal contact of the Almagro B member (AB) is unconformable, with up-section and up-dip decreasing dip of strata from 90 to 55°. This progressive unconformity is caused by the continuous tilt of the strata, resulting from eastward growth of the intrabasinal anticline. (b) The paraconcordant contact, younging to the left (W; see the arrow), between the AgC and AA. A 1-m-thick paleosol developed atop of the AgC. This paleosol can be traced along strike for >10 km northward, in the quebrada Chacra Hualco. The Almagro A member is here represented by a very coarse, monogenetic volcanic breccia interpreted as a primary volcanic block-and-ash flow deposit. It shows a finer and matrix-rich sole-bed. Hammer is 30 cm long. (c) Detail of the stratified tuffaceous mudstone and siltstone bed (tuffite) overlying the clay-rich, massive, reddish paleosol within the AgC. The strata dip is subvertical (85°) and W-dipping (N280° E). The arrow shows the upward sense of the stratigraphic sequence.

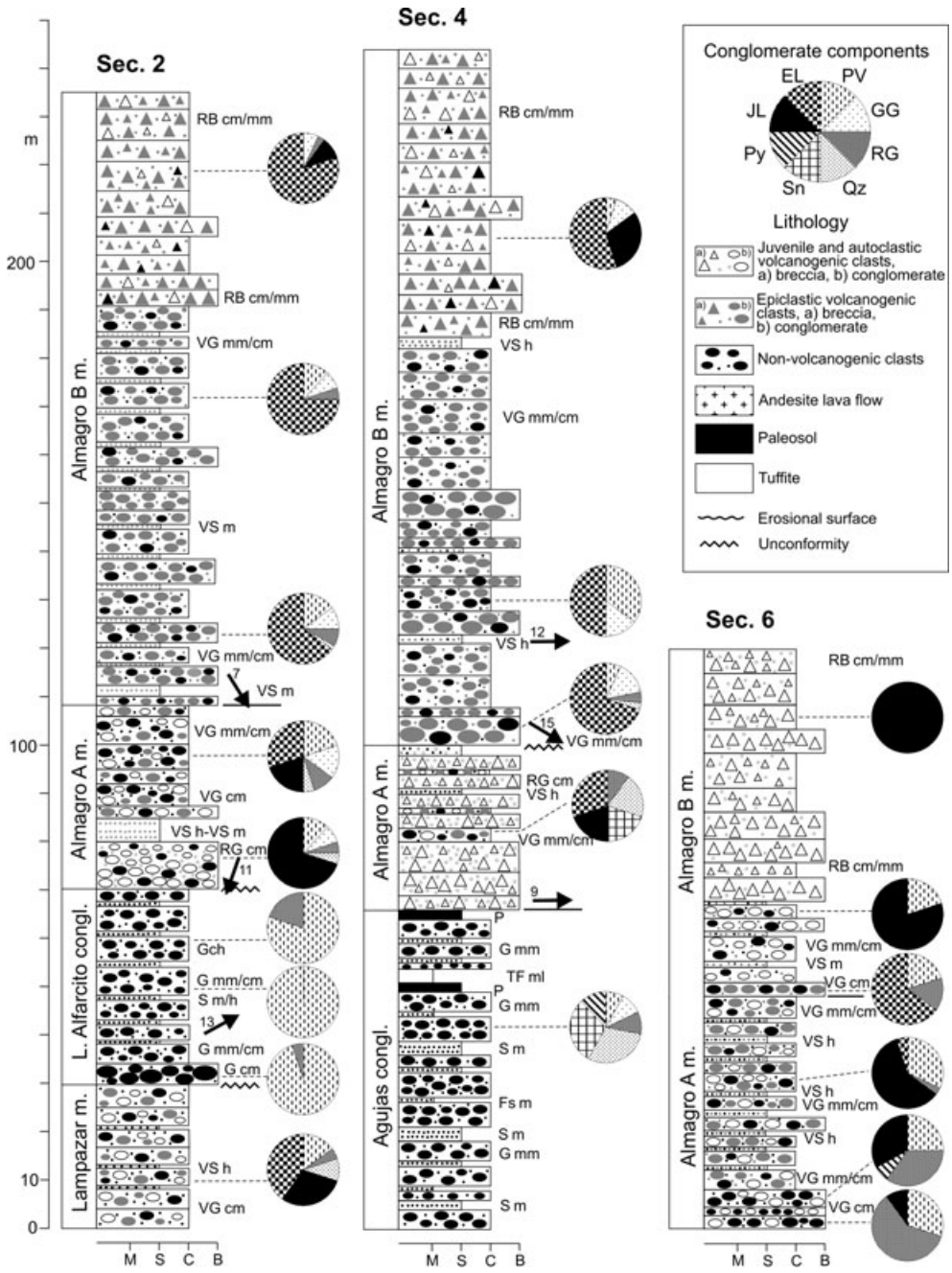

Fig. 4. Measured stratigraphic sections at quebrada Carachi (Section 2), quebrada El Chorro (Section 4) and quebrada Lagunillas outflow (Section 6). Locations are shown in Fig. 2. Pie charts depict conglomerate and breccia petrofacies. Conglomerate components: EL, epiclastic lavas; GG, grey granodiorite; JL, juvenile fragments and autoclastic lavas; PV, siltstone; Py, porphyry; Qz, quartzite; RG, red granite; Sn, sandstone. Grain sizes: M, mud to fine sand; S, sand; C, conglomerate; B, boulder conglomerate. Lithofacies codes as in Table 1. Arrows show paleocurrent directions, where N is taken as the top of the figure (pebble imbrications, the number of measurements is noted on the side).

epiclastic fragmentation. They were transported and deposited from non-cohesive debris flows, transitional to hyperconcentrated flows, reworking coeval volcanic rocks (Pierson & Scott, 1985; Smith, 1986; Zernack *et al.*, 2009). The Las Cuevas member represents the product of explosion and disruption of andesite lava domes in a depositional environment evolving from subaerial to shallow-water lacustrine and alluvial. Related volcanic edifices were located nearby but outside the present outcrop area.

Lampazar member

The Lampazar member (Section 2; Figs 2 and 6) is 7.87 ± 0.17 Ma (Mazzuoli *et al.*, 2008) and composed of volcanogenic conglomerate and sandstone facies (VGcm and VSh; Table 1 and Fig. 4) interstratified in massive-to-diffusely planar-layered beds, 0.5–3 m thick, and intruded by coherent andesite developing peperite facies (Vezzoli *et al.*, 2009).

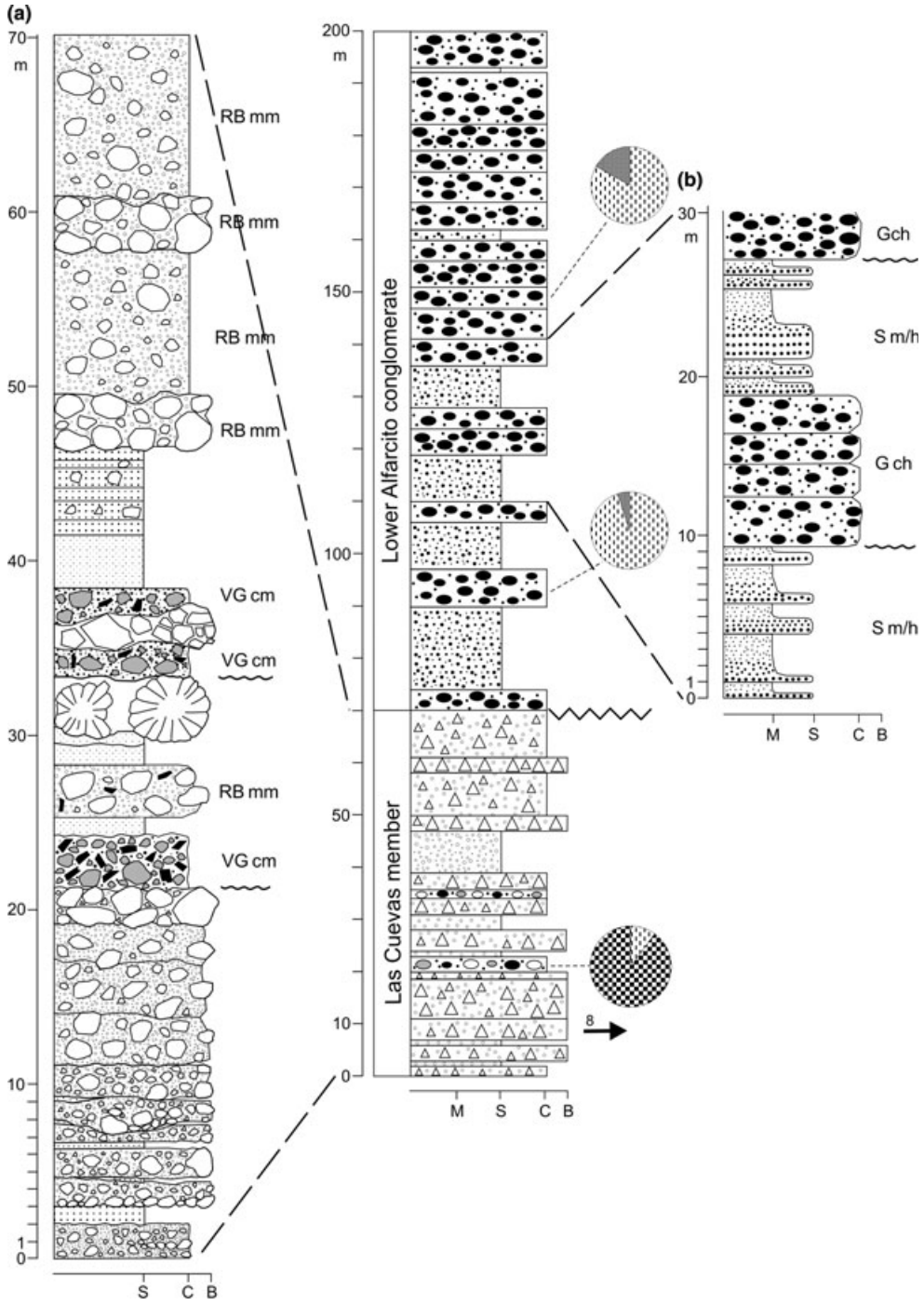

Fig. 5. Measured Section 1 near the Alfarcito village. See Fig. 2 for location map. Stratigraphy and lithofacies of the Las Cuevas member and lower Alfarcito conglomerate are detailed in the (a) and (b) logs respectively. Note the change of log scale. Pie charts depict conglomerate and breccia petrofacies. Lithofacies codes as in Table 1. Grain sizes, conglomerate components and lithology legend as in Fig. 4. Arrows show paleocurrent directions, where N is taken as the top of the figure (pebble imbrications, the number of measurements is noted on the side).

Interpretation

The volcanogenic conglomerate facies (VGcm) represents volcanic materials transported and deposited from subaerial or subaqueous debris flows, reworking basement rocks from older stream deposits and volcanic rocks shortly after intrabasinal eruptions (Zernack *et al.*, 2009). The planar- and cross-lamination and the lenticular and poorly defined beds of the sandstone facies (VSh) may account for stream flows in ephemeral channels reworking the top of the debris-flow deposits. The coherent andesite intrusion, together with volcanogenic clasts in the conglomerate, suggests a volcanic centre near the present exposures of the Lampazar member in the quebrada Carachi.

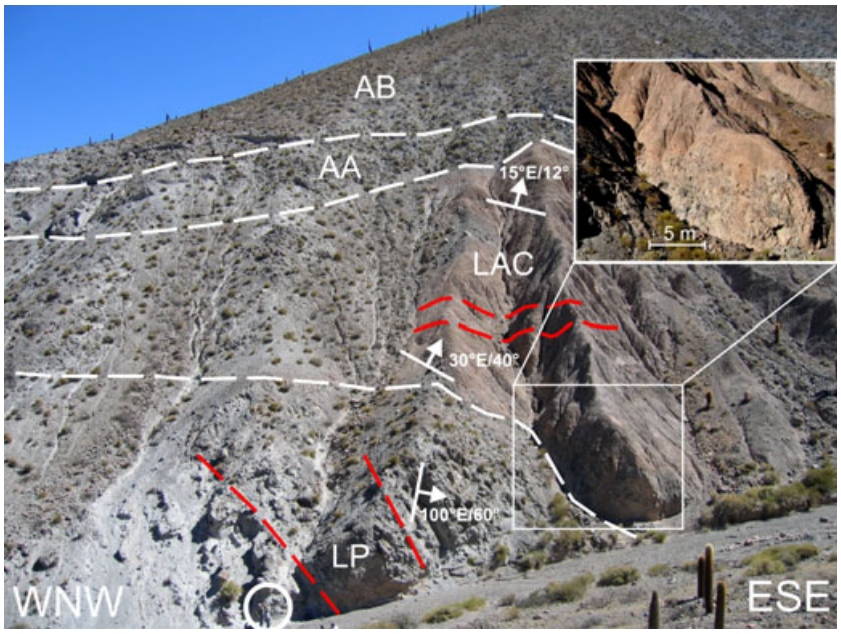

Fig. 6. The stratigraphic transect measured at quebrada Carachi (Section 2 in Fig. 2) showing the interposition of the non-volcanogenic lower Alfarcito conglomerate (LAC) between Lampazar (LP) and Almagro A (AA) volcanic members. The deposition of lower Alfarcito conglomerate started with a boulder conglomerate (Gcm facies) on an erosive surface (detail in the inset). A major angular unconformity separates the LAC and Lampazar member (see dip direction and dip of strata; dashed red lines highlight the intersection of strata with topography). Encircled persons are in foreground to scale. AB, Almagro B member.

Lower Alfarcito conglomerate

The lower Alfarcito conglomerate (Sections 1, 2 and 8; Figs 2, 6, 8, S1B, and S2) consists of stacked, non-volcanogenic, dark grey conglomerate facies (Gmm/cm, Gch and Gcm; Table 1 and Figs 4, 5 and 7) in beds extending laterally for tens to hundreds of metres and arranged in 3- to 30-m-thick units. They are separated by laterally continuous intervals of multiple, planar, normally graded beds with an upward fining texture from tan, massive or rarely horizontally laminated sandstone with occasional scattered pebbles to pale red, massive siltstone and mudstone (Sm/h; Table 1 and Figs 4, 5 and S2). The proportion of the conglomerate facies increases and its grain size decreases upwards and eastwards. Based on its stratigraphic relationships (Section 2; Fig. 4), the age of Alfarcito conglomerate is constrained between 7.87 ± 0.17 and 7.20 ± 0.11 Ma (Mazzuoli *et al.*, 2008). Thickness of the unit is between 30 and 120 m, because of the irregular top and bottom surfaces.

Interpretation

The lower Alfarcito conglomerate facies association suggests an alluvial fan depositional system, dominated by non-cohesive debris flows and sheet floods. The cobble–pebble conglomerate facies (Gmm/cm) accounts for a deposition by laminar, sandy debris flow (Nemec & Steel, 1984; Schultz, 1984). The horizontal stratification of the granule–cobble conglomerate facies (Gch) is interpreted as a result of hyperconcentrated flows (Pierson & Costa, 1987). The coarse and clast-supported (Gcm) conglomerate facies fills channel scours, reworking the debris-flow deposits. Paleocurrent data indicate eastward and northeastward clast transport directions in the Alfarcito (Fig. 5) and Carachi sections (Fig. 4) respectively. The massive-to-poorly stratified sandstone facies (Sm/h) is attributed to hyperconcentrated flows and moderate sediment concentration water flows. The overall tabular geometry of the conglomerate and sandstone beds indicates that the debris flows and sediment-rich water flows were unconfined and sheet-like. The lack of cross-stratification and the scarcity of channel structures suggest that alluvial fans did not have well-developed channel entrenchments.

Almagro A member

The Almagro A member (7.20 ± 0.11 Ma; Mazzuoli *et al.*, 2008) comprises primary volcanic breccia and pumice-rich tuff facies that are interbedded with volcanogenic pebble-boulder conglomerate facies (RGcm, VGmm/cm and VGcm) and sandstone facies (VSh and VSm) (Table 1 and Figs 4, 7 and S3). In both the NW-SE- and SW-NE-oriented transects, the Almagro A member exhibits lateral changes in thickness, geometry of the basal contact and lithofacies distribution and association (Figs 3 and S3). Depositional characteristics vary from proximal and prevailing primary volcanic facies, 20–50 m thick, in the Almagro range (Fig. 7), to distal and resedimented syneruptive and volcanogenic sedimentary facies, 80–100 m thick, in the El Toro basin (Fig. 4).

Interpretation

We propose a syneruptive resedimentation of the RGcm conglomerate facies by channelised debris flows and high-competency water flow (Pierson & Scott, 1985; Smith & Lowe, 1991) of quench-fragmented lavas that mixed with

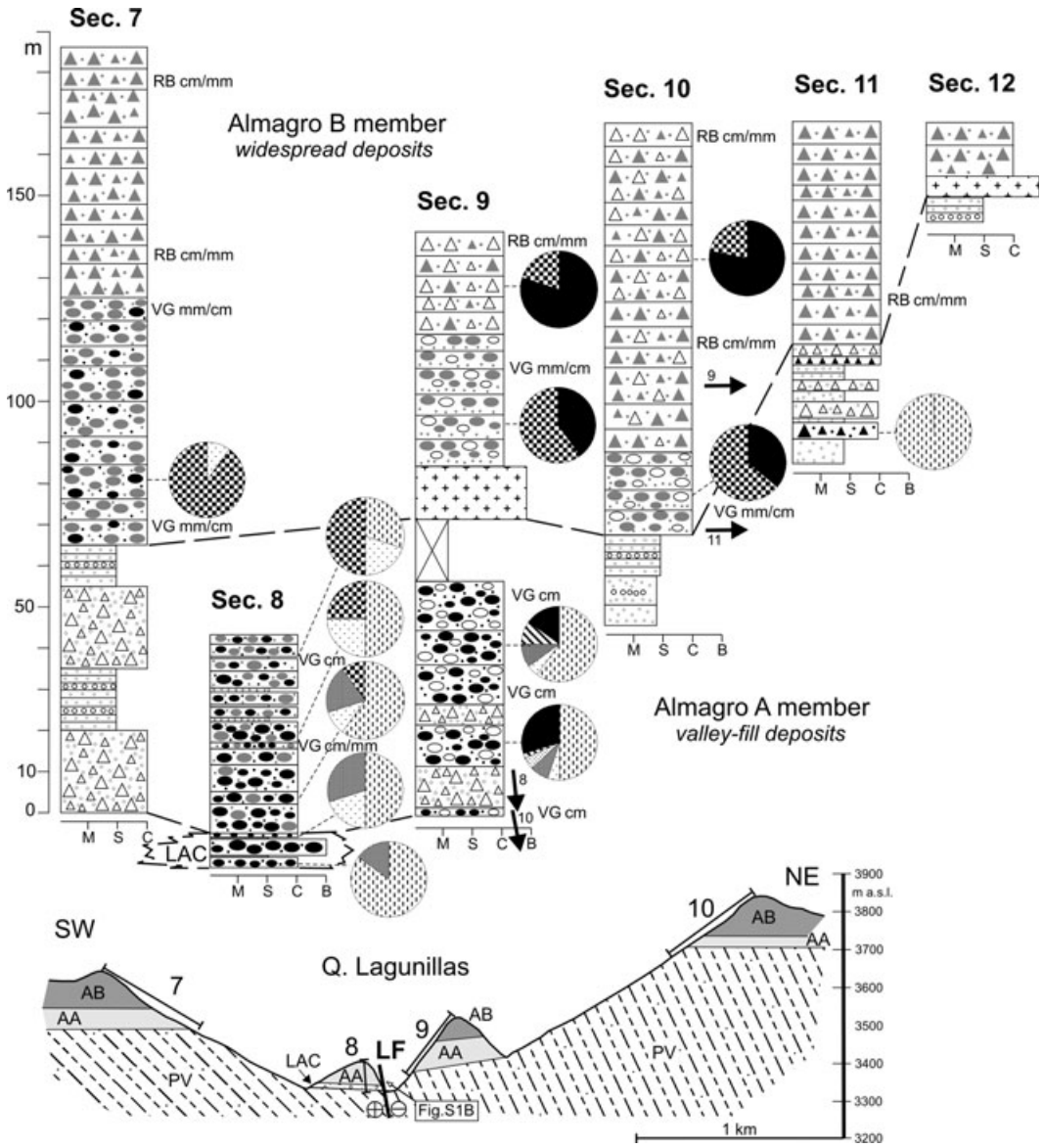

Fig. 7. Measured sections and along-strike stratigraphic correlations showing vertical and lateral facies relations within the interbedded pyroclastic, lava flow and alluvial deposits of the Almagro A and B members in a transect across the quebrada Lagunillas (Almagro range; see Fig. 2 for location). Note that the Almagro A (AA) deposits show different thickness and lithofacies and fill a paleovalley incised into the Puncoviscana Formation (PV), whereas Almagro B (AB) deposits level the paleotopography with a sub-horizontal, widespread and homogeneous lithofacies. Bottom of all logs is PV. In Section 8, the basal non-volcanogenic conglomerate unit is attributed to the LAC (see Fig. S1B). Pie charts depict conglomerate and breccia petrofacies. Lithofacies codes as in Table 1. Grain sizes, conglomerate components and lithology legend as in Fig. 4. Arrows show paleocurrent directions, where N is taken as the top of the figure (pebble imbrications, the number of measurements is noted on the side).

basement clasts. Clast imbrications for this facies record transport directions towards the E (Section 4; Fig. 4) to S (Section 2, Fig. 4; Section 9, Fig. 7). Textures of the volcanogenic sedimentary pebble-boulder conglomerate facies (VGmm/cm) suggest deposition by unconfined debris flows and sheet floods (Blair & McPherson, 1994). The clast-supported pebble-boulder conglomerate facies (VGcm) and sandstone facies (VSh and VSm) resulted from deposition from broad, ephemeral streams reworking debris flow deposits (Blair, 1999). In the Almagro range, lenticular interbeds of non-volcanogenic, clast-supported, massive breccia facies (Bcm; Table 1 and Fig. 7) represent local talus debris.

Almagro B member

The Almagro B member (7.37 ± 0.11 to 6.95 ± 0.10 Ma; Mazzuoli *et al.*, 2008) comprises resedimented syneruptive breccias (RBcm/mm) and volcanogenic conglomerate (VGmm/cm) facies (Table 1; Figs 4, 7 and S4). Discontinuous layers of volcanogenic siltstone and sandstone facies (VSm and VSh; Table 1) drape the coarser beds.

Volcanogenic conglomerate facies (VGmm/cm) prevails in the lower part of the studied distal deposits, whereas syneruptive breccia facies (RBcm/mm) is common closer to western volcanic sources (Fig. 2) and is a significant component of the upper part of the distal exposures (Figs 4 and 7). Conglomerate and breccia facies are arranged in horizontally stratified, stacked successions, 10–40 m thick. In general, individual beds exhibit planar surfaces, non-erosive basal contacts and extend laterally for hundreds of metres. In the quebrada El Chorro (Section 4; Fig. 4), the entire unit is 140 m thick, whereas elsewhere the thickness varies from 160 to 20 m (Figs 4 and 7).

Interpretation

The breccia and conglomerate facies of the Almagro B member are attributed to deposition by unconfined, non-cohesive debris-avalanche and debris flows (Pierson, 1980; Hubert & Filipov, 1989) transitional to hyperconcentrated flows (Pierson & Scott, 1985). Local lenticular sandstone beds with low-angle cross-stratification and conglomerate beds with erosional base and imbricated clasts are interpreted as surface reworking of debris-flow deposits by ephemeral stream flows. Paleocurrent data indicate eastward and southeastward flow (Sections 2 and 4; Fig. 4; Section 10; Fig. 7).

Almagro C member

The Almagro C member (6.7–6.4 Ma; Mazzuoli *et al.*, 2008) comprises andesite, trachydacite and dacite domes and flows (Fig. 2). Feeder dykes trend N–S and WNW–ESE. On the N side of the quebrada Lagunillas, a cluster of cryptodomes intruded, deformed and uplifted the Puncoviscana Formation and the Almagro A and B members.

CONGLOMERATE COMPOSITION AND PROVENANCE

Composition analysis

Each lithostratigraphic unit is characterised by a distinctive conglomerate petrofacies. The composition of clasts, identified in terms of source formations, is depicted in Figs 4, 5 and 7. Clasts of the Las Burras monzogranite were not found on the studied Miocene deposits.

The Agujas conglomerate is non-volcanogenic and composed of whitish and pink quartzite (Meson Group), greenish sandstone (Santa Victoria Group), dark grey siltstone and sandstone (Puncoviscana Formation) and subordinate red granite, dark grey biotite-phyric porphyry and grey granodiorite (Tastil batholith) (Fig. 4).

All the clasts composing the RBmm facies of the Las Cuevas member (Fig. 5) consists of fresh, juvenile, vitrophyric andesite clasts with fluidal shape and quenching textures (i.e. radial fractures, breadcrust surface, glassy margins and contractional cracks). These clasts derived from primary volcanic (autoclastic and pyroclastic) fragmentation. The VGcm facies is polygenetic (Fig. 5) and comprises texturally diverse, non-juvenile andesite lavas and subordinate (10%) subangular clasts of black siltstone (Puncoviscana Formation). These basement rocks were probably sourced by an adjacent talus detritus and were incorporated during the sediment gravity-flow scour.

In the Lampazar member, pebbly sandstone and conglomerate are composed of sub-angular volcanogenic clasts and well-rounded pebbles and cobbles of basement rocks. Volcanogenic clasts comprise different types of lava (amphibole-phyric andesite, clinopyroxene-phyric andesite), pumice and scoria. The modal composition of the basement clasts is dark grey siltstone (Puncoviscana Formation), pinkish quartzite (Meson Group) and red granite and grey granodiorite (Tastil batholith) (Fig. 4).

The lower Alfarcito conglomerate is compositionally homogeneous and dominated (95–70%) by platy, sub-angular fragments of dark grey siltstone derived from the Puncoviscana Formation. A subordinate amount (maximum 30%) of sub-rounded, red granite pebbles was derived from the Tastil batholith (Figs 4 and 5). Clasts of volcanic origin are absent.

In the Almagro A member, polygenetic sedimentary conglomerates are interbebbed with monogenetic volcanic breccias. These deposits show an upsection progressive decrease in basement components and an increase in primary volcanic clasts (Fig. 7). Volcanic clasts comprise pale-grey to pink, microvesicular amphibole-phyric andesite; subordinate lava clast types are black scoriaceous andesite and plagioclase-phyric andesite. In the RGcm facies, several lava clasts show radial and concentric joints, glassy quenched rims, and are often fractured with jigsaw cracks filled with the vitric ashy matrix (Fig. S3D). The basement-derived conglomerate clasts are very well rounded and composed of quartzite (Meson Group) and dark grey siltstone (Puncoviscana Formation) (Figs 4 and 7).

Our data from the Almagro B member indicate an upward enrichment of juvenile and autoclastic fresh lava clasts relative to non-juvenile lava and basement clasts. Volcanic clasts mainly comprise clinopyroxene-phyric grey andesite, plagioclase-phyric dark grey andesite and red and black vitrophyric andesite breccia. The basement clasts are composed of abundant red granite and grey granodiorite (Tastil batholith), minor siltstone (Puscoviscana Formation) and subordinate quartzite (Meson Group) (Figs 4 and 7).

Provenance interpretation

Composition analysis and lithologic provenance modelling for conglomerate clasts suggest the following: (a) primary source areas were all western domains; (b) the source stratigraphy comprises the Neoproterozoic through Paleogene rocks of the Eastern Cordillera and Miocene intrabasinal volcanics; (c) source lithologies

become older stratigraphically higher in the sequence; (d) volcanic activity is synchronous with the basin sedimentary evolution; (e) volcanic sources alternate with basement sources and (f) intrabasinal Neogene deposits were cannibalised and recycled into younger units.

Our data constrain the westward provenance (the actual eastern border of the Puna plateau and Almagro range) and exclude an eastern provenance (Sierra de Pasha) as supported by the following evidence. Firstly, any detritus from the Tastil intrusive rocks must have come from the Almagro range, as the eastern ranges do not contain these rocks (Fig. 1). Secondly, on Sierra de Pasha, the Paleozoic strata show a minimal erosion, and the complete sequence of the Puncoviscana Formation is exposed at the base of the hangingwall of the Golgota Fault (Fig. 1). Finally, the paleocurrent directions measured in this study (Figs 4, 5 and 7) and previously reported (Marrett & Strecker, 2000; Hilley & Strecker, 2005) indicate that conglomerate clasts were shed from a source area W of the basin.

The early Almagro–El Toro deposition was dominated by sandy and silty alluvial systems. Conglomerate did not develop, probably because coarse detritus was not available. The only rock types of the source section that do not yield coarse detritus when weathered are the reddish mudstone and sandstone of the Cretaceous–Paleogene Salta Group. The red mudstone and siltstone of the lowest Neogene sedimentary unit (Barres sandstone) were probably derived primarily from the Salta Group rocks. The coarse alluvial fan sedimentation commenced with the exposure and unroofing of the durable Paleozoic rocks. The lowest conglomerate unit (Agujas conglomerate) abounds in quartzite and sandstone clasts derived from the lower Paleozoic part of the source section. Stratigraphically higher samples are progressively enriched in Neoproterozoic-Cambrian low-metamorphic and intrusive basement clasts (Figs 4 and 7).

Equigranular and subangular clast textures of the medial part of the Almagro–El Toro basin fill (Agujas conglomerate) indicate a first-order provenance from the erosion of primary basement source areas. Mixed clasts with different compositions and mechanical behaviour and the well-rounded textures of the basement pebbles in the upper part of the sequence (Lampazar, Almagro A and B members) suggest the potential recycling of the partially cannibalised basement clasts from older intrabasinal Neogene units (probably the Agujas conglomerate or equivalents) (Zernack *et al.*, 2009). The first-order origin suggests tectonic events that produced exhumation, rock uplift and erosion of basement-cored thrust slices, whereas recycling implies thrust front migration and intrabasinal tectonic deformations.

The clast composition of the lower Alfarcito conglomerate indicates derivation from the erosion of adjacent domains (Almagro range; Fig. 1). The restricted areal distribution (Fig. 2) and the local source areas of the lower Alfarcito conglomerate suggest a first-order provenance. The source area of the Almagro range was already entirely stripped of its Paleozoic–Paleogene cover rocks by the time the lower Alfarcito conglomerate began to accumulate. This is suggested by the following: (a) the absence of clasts from Paleozoic to Paleogene rocks in the conglomerate and (b) the direct contact of Almagro A and B members over the Neoproterozoic-Cambrian basement rocks in the Almagro range (Figs 1 and 2).

By the time of the Almagro A and B deposition, the foreland basin fill interacts with volcanism. Petrographic composition of volcanic members is very distinctive. The low internal clast variability, coarse grain-sized deposits and gravity-flow processes suggest a local provenance from nearby volcanic sources (Smith, 1991; Vallance, 2000; Zernack *et al.*, 2009).

Tectonic and volcanic controls on sedimentation

The association and distribution of the lithofacies of the Almagro–El Toro volcano-sedimentary sequence can be attributed to alluvial fan progradation in response to driving forces, such as tectonic rejuvenation of source-area relief, change in source-area lithology, onset of volcanism and climate variations (DeCelles *et al.*, 1991; Alonso *et al.*, 2006). In the study area, volcaniclastic beds reflect episodic, short-duration sedimentation events associated with volcanism. In the measured sections, the percentage of proximal, primary, volcanic-dominated deposits increases westward. Conversely, the amount of gravel-sheet debris-flow deposits increases eastward. These trends in proximal vs. distal deposition can be explained in terms of a combination of the evolving tectonic setting and changing source lithology.

The primary control on deposition of the Almagro–El Toro sequence was a compressional deformation driving rock uplift, exhumation and denudation. This is indicated by the significant thickness and coarseness of the conglomerate facies, the general upsection coarseness sequence, the predominant proportion of debris flow deposits, and the inverse stratigraphy (unroofing sequence) recorded in clast compositions. Systematically, within each stratigraphic unit, conglomerate grain size trends to be finer upward, and basal beds comprise very coarse boulder conglomerate facies. These coarse alluvial pulses can reflect recurrent structural reactivations of faults with an initial moment of incremental deformation, exhumation and uplift followed by a steady period of alluvial basin filling, mainly produced in response to basin subsidence.

Source lithology exerted a secondary but important control on depositional processes in the Almagro–El Toro basin. First, the source regions show a stratigraphy with upward decreasing durability. Indeed, fine-grained Cretaceous–Paleogene deposits dominated the upper levels, resistant Paleozoic siliciclastic rocks characterised middle levels and the core of the uplift was composed of Neoproterozoic-Cambrian crystalline rocks. This difference in the mechanical properties among source lithologies may

have also induced differences in apparent erosion rate, sediment grain size and transport processes. In other contexts, it has been demonstrated that where young, soft strata overlie a more resistant basement, the appearance of coarse clastic material in the foreland basin can substantially postdate the onset of orogenic deformation and exhumation (Sobel & Strecker, 2003; Deeken *et al.*, 2006).

The effects of volcanism on the Almagro-El Toro depositional system were significant because BAT volcanic activity controlled the depositional timing, environmental distribution and lithologic character (coarse detritus) of the associated sediments. Volcanogenic sedimentary units accumulated during eruptive activity at nearby, co-genetic volcanoes. Noticeably, during the deposition of Almagro A and B members, resedimented syneruptive deposits represent aprons around active volcanoes, grading laterally into accumulations of volcanogenic sediments and non-volcanogenic, mainly secondary detritus (Smith, 1991; Zernack *et al.*, 2009). The transition from syneruptive to intereruptive conditions was abrupt. During intereruptive periods, volcanism had no impact on the depositional system, even as secondary source. Volcanism induced elevated aggradation in alluvial basins (as in the Lagunillas paleovalley; Fig. 7) because of the emplacement of additional debris within the drainage basin and the perturbation of the sediment yield. The main effects of volcanism on the depositional system are the following: (a) changes in the amount of detrital material supplied to the basin from the short-term production of large volumes of autoclastic fragments; (b) changes in the lithology of detrital materials and (c) an increase in the grain size of the deposits. During volcanic episodes, the basement surface was buried under a thick and extensive volcanic cover and the basement rocks were probably inhibited as first-order source units.

STRUCTURAL FEATURES

Interaction between the depositional system and tectonics

Several structural features highlight the deformation history experienced by the Almagro-El Toro foreland basin during the deposition of the middle-upper Miocene volcano-sedimentary sequence. The most meaningful features are the following: (a) the direct superimposition of different Miocene units over different basement rocks; (b) the lack of Cenozoic deposits older than 7.4 Ma in the Almagro range; (c) several time lags in the stratigraphic sequence; (d) the overlap of the Almagro C member on the top of the Las Burras laccolith; (e) intraformational growth strata and (f) intrabasinal unconformities and syndepositional folds and faults.

The San Bernardo Fault (Marrett *et al.*, 1994) thrusts Neoproterozoic-Cambrian basement rocks over upper Miocene non-marine sedimentary and volcanic rocks, truncating the Neogene sequence (Figs 2 and S2). Field relations suggest that fault displacement decreases progressively along strike to the NNE, turning into a monocline fold deforming the Almagro A and B members (Figs 1 and 2). Then, the structure of the W margin of the El Toro basin can be associated with the activity of a fault-propagation fold, involving a core of basement rocks and limb rotation during deposition (e.g. Hardy & Poblet, 1994; Vergés *et al.*, 1996). The oldest unit of the Neogene volcano-sedimentary sequence involved in this deformation (Las Cuevas member; 11.1 Ma) indicates the minimum age of fault activity; however, the unroofing of the Paleozoic-Paleogene hangingwall resulting in the deposition of Barres sandstone and Agujas conglomerate suggests that the fault has been active since *ca.* 12.5 Ma.

Along the San Bernardo Fault, well-preserved examples of interrelations between syntectonic deposition and evolving structures occur, demonstrating that the fault was active during the deposition of the foreland basin strata.

In the footwall of the San Bernardo Fault (Alfarcito; Section 1; Figs 8 and S2), growth strata, the wedge-shape geometry of beds in cross-section and progressive intraformational unconformities reveal the fault motion during the sedimentation of the upper Miocene deposits at 11.1 Ma (Las Cuevas member) and *ca.* 7.5 Ma (lower Alfarcito conglomerate). The Las Cuevas member deposited directly over the Tastil grey granodiorite (Figs 8 and S2) that was exposed and domed prior to the sedimentation. The lower Alfarcito conglomerate rests unconformably on top of Las Cuevas member (Figs 8 and S2) after a non-depositional or erosional hiatus of *ca.* 4 Ma.

In both the Las Cuevas member and lower Alfarcito conglomerate, strata overlap and onlap pre-existing rocks, showing a progressively westward younging at the base (Figs 8 and S2). Moreover, single beds or groups of beds thicken across the exposure from the fault plane eastward, angular unconformities occur between groups of beds and the beds show an upsection decrease in dip from stratigraphically lower to higher strata (Fig. 8). These intraformational progressive unconformities formed when the proximal W part of the depositional body rotated basinward during the fault-propagation folding along the front of the Almagro range (Burbank *et al.*, 1992; Vergés *et al.*, 1996; Carrera & Muñoz, 2008). Finally, in both the Las Cuevas member and lower Alfarcito conglomerate, the onlapping contacts partly coincide with syndepositional NW-striking fault planes (Figs 8 and S2; site 24 in Acocella *et al.*, 2011).

Within the El Toro basin, synsedimentary deformation suggests that the orogenic wedge propagated into the basin fill. Deformations were recorded by unconformities and changes in conglomerate coarseness and petrofacies. A major angular unconformity separated the Lampazar member and the lower Alfarcito conglomerate (Section 2; Fig. 6). The Lampazar member forms the core of an anticline with 50°–70° dip of limb strata. The overlying lower Alfarcito conglomerate is erosive with a basal bed of cobble-boulder conglomerate of basement-derived clasts that

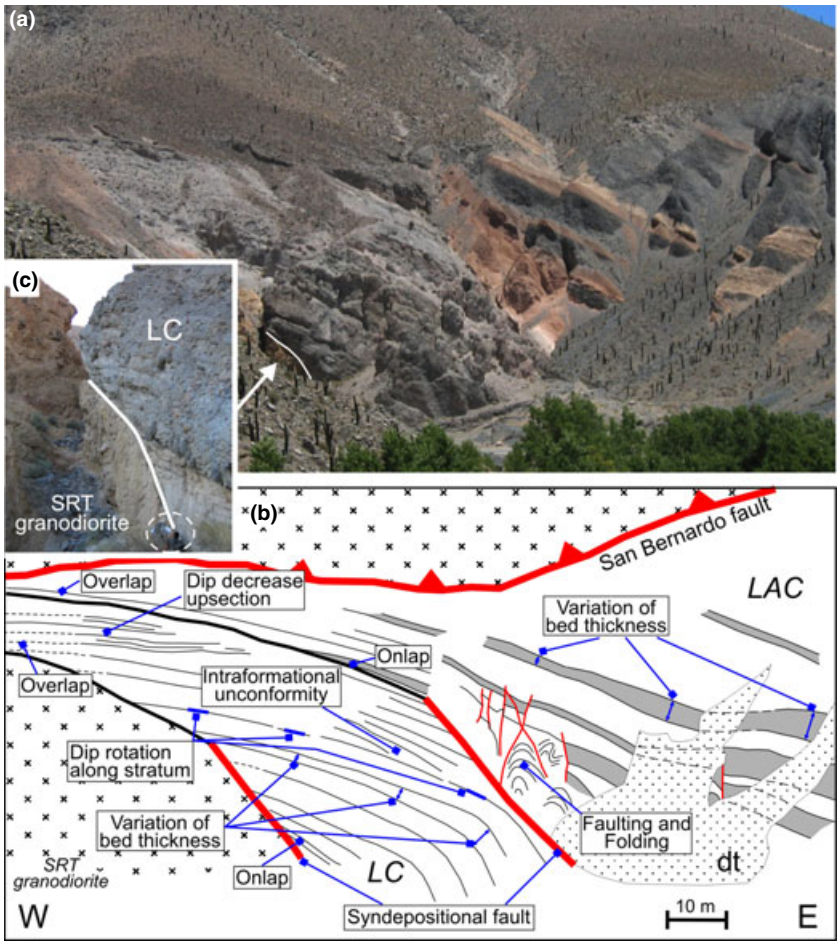

Fig. 8. Photograph (a) and interpretative line drawing (b) of the stratigraphic and tectonic contacts between the Santa Rosa de Tastil granodiorite (SRT), Las Cuevas member (LC) and lower Alfarcito conglomerate (LAC) in the Alfarcito outcrop (Section 1 in Fig. 2; see Fig. S2 for overviews of exposure). Syntectonic deposits preserve several growth stratal structures showing progressive changes of bed dip (stratal rotation) and thickness (stratal thinning), both up-dip and up-section. dt, detritus cover. (C) Close-up on the NW-striking fault (white line) that poses in contact the early Cambrian granodiorite with tuffs and block-and-ash flow deposits of the LC. Encircled persons are in foreground for scale.

truncates the stratification of the Lampazar member (Fig. 6). The dip of the conglomerate strata is 40° near the unconformable contact and decreases upward by 10°–15° (Fig. 6). Folding must have occurred after the deposition of the volcanic rocks and before the deposition of the conglomerate, to explain their angularly unconformable relation. Moreover, the growth of the anticline continued during the conglomerate deposition, as suggested by the progressive flattening of the dip of the layers in the lower Alfarcito conglomerate. Minor low-angle unconformities and erosion surfaces are at the base of the Almagro A member (Fig. S3) and at the contact between the Almagro A and B members (Fig. 3).

Within the Almagro range, the quebrada Lagunillas coincides with the NW-striking Lagunillas Fault (COT fault zone; sites 21 and 36 in Acocella *et al.*, 2011) whose syndepositional strike-slip movements were registered by growth strata in the lower Alfarcito conglomerate (ca. 7.5 Ma; Fig. S1B).

The role of the COT Fault Zone in foreland deformation and volcanic activity

A number of prominent geological and structural observations in the Almagro–El Toro region indicate a tectonic influence of the NW-striking, strike-slip COT fault zone (Acocella *et al.*, 2011) on the foreland basin deposition, BAT magma rise and deformation of the Eastern Cordillera (Fig. 9). Structural data reported by Mazzuoli *et al.* (2008) suggest that the NW-striking faults have probably been active since at least 14 Ma, that is during the emplacement of the Las Burras laccolith.

Direct evidence of the synsedimentary tectonic activity of the NW-striking faults is found in the Alfarcito and Lagunillas exposures. At Alfarcito, the onlapping contacts of both the Las Cuevas member (11.1 Ma) and lower Alfarcito conglomerate (*ca.* 7.5 Ma) partly coincide with syndepositional NW-striking fault planes (Figs 8, 9 and S2; Alfarcito segment of the COT fault zone; site 24 in Acocella *et al.*, 2011). The syndepositional strike-slip movement of the NW-striking Lagunillas Fault (Figs 2 and 9; sites 21 and 36 in Acocella *et al.*, 2011) is recorded by growth strata in the lower Alfarcito conglomerate (*ca.* 7.5 Ma; Fig. S1B). Moreover, several NW-trending feeder dykes of the Almagro A and B members indicate that the observed transtensive motion along the COT fault zone (Acocella *et al.*, 2011) probably provided favourable conditions for the rise and emplacement of BAT magmas (Fig. 9).

A further and indirect suggestion of the driving control of the COT fault zone derives from differences in the evolution of the El Toro basin after the deposition of the

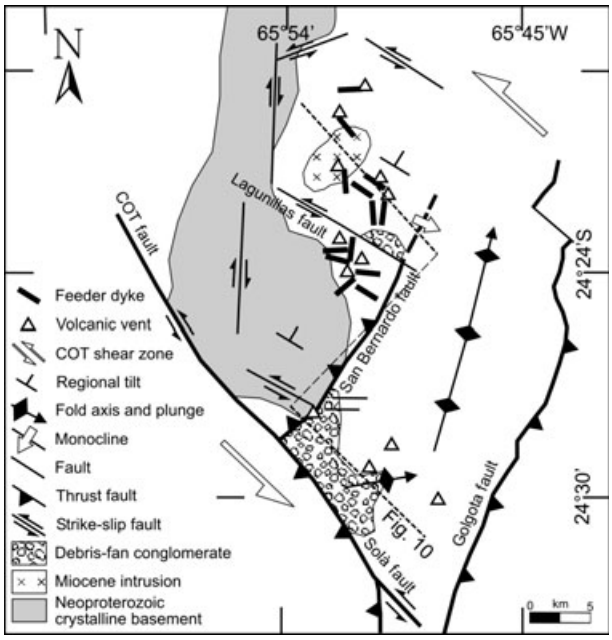

Fig. 9. Sketch map of tectonic, depositional and volcanic structures along the easternmost segment of the COT fault zone. Location as in Fig. 1. The hashed line indicates the transect shown in Fig. 10.

Agujas conglomerate. At this time, the N part of the basin experienced a limited sediment accumulation and a tectonic quiescence, as indicated by the following: (a) the pedogenetic alteration of the material exposed on the floodplain and alluvial fan surfaces, atop of the Agujas conglomerate (Fig. 3); (b) the absence of deposits with ages between *ca.* 11 and 7.2 Ma (Fig. 2); (c) the deposition in low-gradient environments (lacustrine tuffite) (Fig. 3c) and (d) the paraconformable contact with the Almagro A member (Fig. 3b). Conversely, the southern basin margin, near the Alfarcito-Solá segment of the COT fault zone, focused volcanic vents (Las Cuevas and Lampazar members), intrabasinal deformations and alluvial fan depocentres (lower Alfarcito conglomerate) (Figs 2, 9 and S1B). In particular, the composition of clasts and paleocurrent directions (towards E and NE; Figs 4 and 5) of the lower Alfarcito conglomerate suggest that the related alluvial fans probably developed locally, fed by the active fault scarps of the Alfarcito, Solá (Marrett & Strecker, 2000) and Lagunillas Faults.

Finally, uplift may have locally been associated with strike-slip tectonics (e.g. Wilcox *et al.*, 1973; Sylvester, 1988; Fossen & Tikoff, 1998; Spotila *et al.*, 2001). We speculate that the strike-slip tectonic activity along the COT fault zone, together with the inherited paleogeographic and structural pre-Andean features of this lineament (Allmendinger *et al.*, 1983; Kley *et al.*, 1999), induced a heterogeneous crustal response to the orogenic deformation. The diachronous and spatially variable tilting and exhumation of the NE sector of the COT fault zone may be depicted by the along-strike evolution of the fold related to the San Bernardo Fault (Fig. 9; Salvini & Storti, 2002). The differential deformation probably commenced in the SW with the earliest exhumation of the Tastil batholith prior to 11.1 Ma and propagated NE into a syndepositional monocline fold, deforming the Almagro A and B members (Figs 1 and 2). In a similar way, the Lagunillas Fault may have driven the differential tilting and exhumation of the basement block containing the Las Burras laccolith (Fig. 9).

DEPOSITIONAL HISTORY AND TECTONIC IMPLICATIONS

Our results suggest that the Almagro-El Toro region evolved as a synsedimentary deforming foreland depositional system during the middle to late Miocene. Its spatial and temporal evolution in response to sedimentary, tectonic and volcanic processes is summarised in Fig. 10. The sediment accumulation rate and exhumation history are shown in Fig. 10f. The total thickness of the exhumed source section is estimated at *ca.* 6.5 km. Conglomerate clast composition suggests which stratigraphic level was exposed and unroofed during the exhumation. Exhumation rates were evaluated by dated volcanic members and the inferred age of the interbedded sedimentary rocks.

The onset of magmatism is represented by the intrusion of the Las Burras laccolith at 14.3 Ma (Figs 2 and 10a), emplaced at a maximum depth of 6.5 km. No geologic record of the paleogeographic setting, sedimentation and volcanism coeval with the Las Burras emplacement was preserved in the Almagro range.

The basal part of the El Toro volcano-sedimentary sequence (Barres sandstone) was deposited on a distal alluvial fan and floodplain system dominated by sheet flows and overbank floods. Magmatism with geochemical and isotopic signatures similar to the Las Burras intrusion (Mazzuoli *et al.*, 2008) continued with the andesitic lava flows of the Puerta Tastil member (12.8 Ma), (Fig. 10a).

The lack of dated horizons in the basal part of the volcano-sedimentary sequence prevents a direct time correlation between the Las Burras intrusion and early depositional events on the El Toro basin. Considering a typical sedimentation rate for a foredeep depozone of 0.3 ± 0.1 mm a^{-1} (Viramonte *et al.*, 1994; Reynolds *et al.*, 2000; DeCelles & Horton, 2003) and the accumulation rate of 0.23 mm a^{-1} estimated in Fig. 10f, we infer an age of 13.7 ± 0.4 Ma for the onset of basin filling. Fine-grained sediments of the Barres sandstone may be sourced by the Salta Group red beds. This implies that the region between the eastern Puna plateau and the Almagro range was already exhumed (at a rate of 1.66 mm a^{-1}; Fig. 10f) and uplifted as a result of the incipient formation of the Eastern Cordillera orogenic wedge (Fig. 10a). The depositional system was probably able to bypass the deforming zone and deposit finer sediments in distal portions.

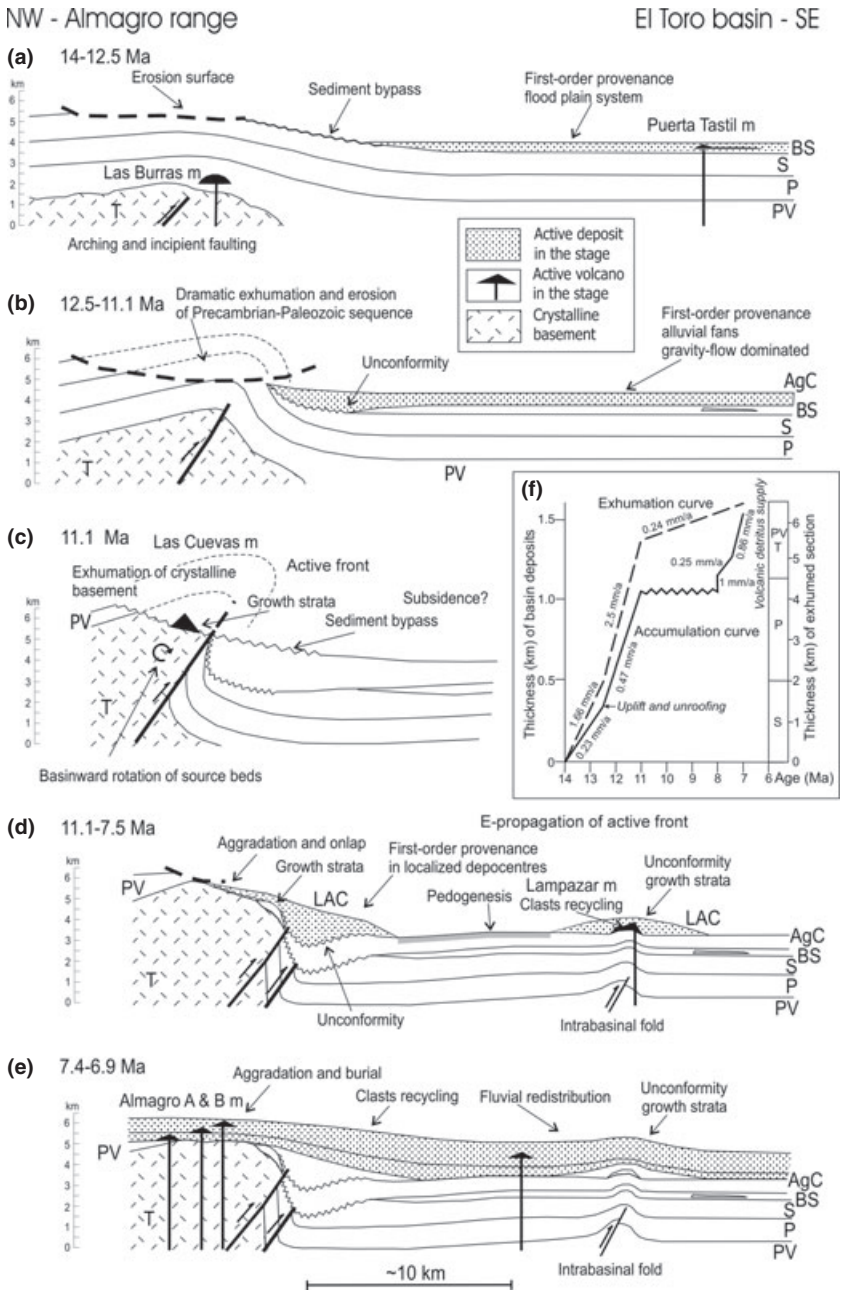

Fig. 10. Schematic evolution of the Almagro-El Toro foreland basin in a NW–SE cross-section (location as in Figs 1, 2 and 9). The present distance between the Almagro range and the El Toro basin is *ca*. 30 km; horizontal shortening is not to scale. The sequential restorations (a–e) are in order of decreasing age. (a) Fine-grained sheet flood deposits on a regional planation surface fed by erosion of red beds of the Salta Group on a broad regional arching. The Las Burras laccolith may have emplaced on this arching. (b) The first conglomerate unit records the basement thrusting, exhumation and erosion along the San Bernardo Fault. (c) Differential uplift exposed crystalline basement. Note that the Las Cuevas member is incorporated into a growing anticline of the San Bernardo Fault. (d) Localised deposition of volcanic products and conglomerates. The deformation propagated to an intrabasinal anticline. (e) Deposition of andesite volcanism of the Almagro A and B members. (f) Sediment accumulation and exhumation history for the Almagro-El Toro deposits using measured thicknesses. The diagram shows the onset of the main phase of exhumation and unroofing at 12.5–11.1 Ma, hiatus in sedimentation at 11.1–7.8 Ma and strong influx of volcanic detritus after 7.8 Ma. AgC, Agujas conglomerate, BS, Barres sandstones, LAC, lower Alfarcito conglomerate, P, Paleozoic units, PV, Puncoviscana Formation, S, Salta Group, T, Tastil batholith.

By *ca*. 12.5 Ma, the flood-plain system evolved into a complex of primary-sourced, debris flow-dominated alluvial fans (Agujas conglomerate; Fig. 10b) with the influx of a large amount of westerly sourced, Neoproterozoic to Paleozoic clasts. The sediment accumulation rate (0.47 mm a^{-1}) doubled with respect to the previous phase (Fig. 10f). Drainage was predominantly eastwards, across the axis of the foreland basin; however, lithofacies do not highlight any distinct drainage outlet along the orogenic front. During this episode (12.5–11.1 Ma), (1) the main deformation along the San Bernardo fault occurred (Fig. 10b); (2) the primary-sourced clasts of the Agujas conglomerate and the overlap of the Las Cuevas member on the Tastil batholith suggest that the SW sector of the Almagro range was stripped of at least 3.5 km of its sedimentary cover and (3) the exhumation rate reached 2.5 mm a^{-1} (Fig. 10f).

After the deposition of the Agujas conglomerate (11.1–7.5 Ma), a stable non-sedimentation phase dominated in the N side of the basin over *ca*. 4 Ma (Fig. 10c, f). The absence of deposits of this age on the Almagro range may be related to recycling of foreland deposits and/or bypass of sediments eastwards into distal depositional systems. In contrast, on the S side of the basin, deposition was episodically controlled by (a) spotted volcanism (Las Cuevas member, 11.1 Ma; Lampazar member, 7.9 Ma), (b) cannibalisation of middle Miocene conglomerates (Lampazar member) and (c) localised depocentres of coarse-grained primary-sourced sedimentation (lower Alfarcito conglomerate) (Fig. 10c, d).

Moreover, the S part of the basin records three episodes of syndepositional tectonics as intrabasinal deformations and unconformities. The first evidence of intrabasinal tectonic activity was the growth strata on the Las Cuevas member (11.1 Ma) and their onlapping relations with the deforming and exhumating Tastil granodiorite (Figs 8, 10c and S2). Subsequently, beds of the Lampazar member (7.9 Ma) record the onset of the activity of intraforeland structures (Figs 6 and 10d). This unit was folded and tilted into an ENE-trending anticline above an active blind thrust, just prior to the deposition of the non-volcanogenic lower Alfarcito conglomerate. Finally, the lower Alfarcito conglomerate (*ca.* 7.5 Ma) shows syndepositional tectonic deformation and growth strata at Alfarcito (the belt front along the San Bernardo Fault), quebrada Carachi (the intrabasinal anticline) and quebrada Lagunillas (the NW-striking, strike-slip fault) (Figs 8, 10d, S1A and S2). Structural and sedimentologic differences along the N and S sides of the Almagro–El Toro basin suggest that tectonic deformation and exhumation of the orogenic front differentiated along-strike, with intrabasinal deformation, volcanism, conglomerate production and uplift focused on the Alfarcito–Carachi and Lagunillas areas (Fig. 9).

The late-stage fill of the Almagro–El Toro basin (7.5–6.9 Ma; Almagro A and B members) is dominated by volcanogenic boulder- and cobble-sized conglomerate and breccia, from a debris flow-dominated, proximal to middle alluvial-fan setting, interbedded with primary volcanic facies (Fig. 10e, f). At each unit contact, the sequence coarsens abruptly. Volcanic centres focused on the Almagro range, near the quebrada Lagunillas; some vents are present within the El Toro basin (Figs 2 and 9). During this volcanic phase, orogenic shortening appears less active, the exhumation rate significantly decreases (0.24 mm a^{-1}; Fig. 10f) and the accumulation rate increases at 1–0.86 mm a^{-1} (Fig. 10f), as a consequence of the volcanic detritus supply. Evidence of syndepositional tectonics along the intrabasinal folds was recorded from the unconformable basal contacts of both the Almagro A and B members (Fig. 10e). Basement-derived clasts in conglomerates were quasi-exclusively furnished by reworking of the previously deposited middle Miocene strata, suggesting that foreland sediments were locally involved within the thrust system, becoming a source area.

Finally, after the deposition of the Almagro B member (6.9 Ma), the middle Miocene Las Burras laccolith was exposed to the topographic surface and covered by lavas of Almagro C member (6.7–6.4 Ma; Mazzuoli *et al.*, 2008). Subsequently, during the Pliocene-Quaternary, the depositional system of the Almagro–El Toro basin was separated from the active foreland by the surface uplift of the Almagro range and the Sierra de Pasha and became a contractional basin incorporated into the orogen (Marrett & Strecker, 2000; Hilley & Strecker, 2005).

MIOCENE EVOLUTION OF THE CENTRAL ANDEAN FORELAND BASIN

Regional stratigraphy

The regional correlation of the Tertiary stratigraphic record along a transect at *ca.* 24° S is presented in Fig. 11. This correlation is crucial to the reconstruction of the evolution of the Andean foreland basin system during the middle Miocene–Pliocene. Sediments are preserved (Fig. 11a) in the intermontane basins within the Puna plateau (Salars de Arizaro and Pastos Grandes; Alonso, 1992; Vandervoort *et al.*, 1995) and Eastern Cordillera (Calchaquí Valley; Carrera & Muñoz, 2008; Almagro–El Toro basin; Marrett & Strecker, 2000; Hilley & Strecker, 2005; this article) and in the thick sedimentary cover of the Santa Barbara System (Rio Yacones; Viramonte *et al.*, 1994; Arroyo Gonzalez; Gebhard *et al.*, 1974; Reynolds *et al.*, 2000).

Middle Eocene and Oligocene non-marine clastic sedimentary rocks are exposed on the Puna plateau (Geste Formation; Alonso, 1992; Vandervoort *et al.*, 1995; Coutand *et al.*, 2001; DeCelles *et al.*, 2007) and on the southern Eastern Cordillera (Quebrada de los Colorados Formation; Starck & Anzótegui, 2001; Hongn *et al.*, 2007; Carrera & Muñoz, 2008; Fig. 11b). These represent the infill of an initial stage of a foreland basin, and document the timing and distribution of pre-Neogene Andean shortening. The deformation, uplift and erosion developed in the western Puna plateau (the present Western Cordillera and Cordillera de Domeyko). The buried orogenic front was located along the eastern margin of Puna (proto–Eastern Cordillera), as suggested by growth strata and clast provenance directions (Starck & Anzótegui, 2001; Hongn *et al.*, 2007). Moreover, the fission track data from basement-cored ranges (Sierra de Chango Real; Coutand *et al.*, 2001; Tastil batholith; Andriessen & Reutter, 1994; Cumbre de Luracatao; Deeken *et al.*, 2006) suggest rapid cooling and exhumation of the proto–Eastern Cordillera at 38–30 Ma. Further E along the studied transect, in the Eastern Cordillera and Santa Barbara System, Eocene–lower Miocene strata have not been recorded and middle–upper Miocene strata are superimposed on the Salta Group (Fig. 11b).

At *ca.* 24° S, the Neogene sediment accumulation began at *ca.* 15 Ma and was coeval on the Puna plateau and foreland (Eastern Cordillera and Santa Barbara System), although with different facies types and distribution (Fig. 11b). On the Puna, evaporites of internally drained basins dominated the stratigraphic record between 15 and 4 Ma, with limited temporal hiatuses, unconformities and deformations (Vandervoort *et al.*, 1995; Sobel *et al.*, 2003; Payrola Bosio *et al.*, 2009). This suggests that the Puna basin was not feeding the foreland basin, becoming a structurally isolated depositional system because of the uplift of the Eastern Cordillera.

The lithofacies, unconformities and time hiatuses shown in Fig. 11 suggest that the middle Miocene–Pliocene

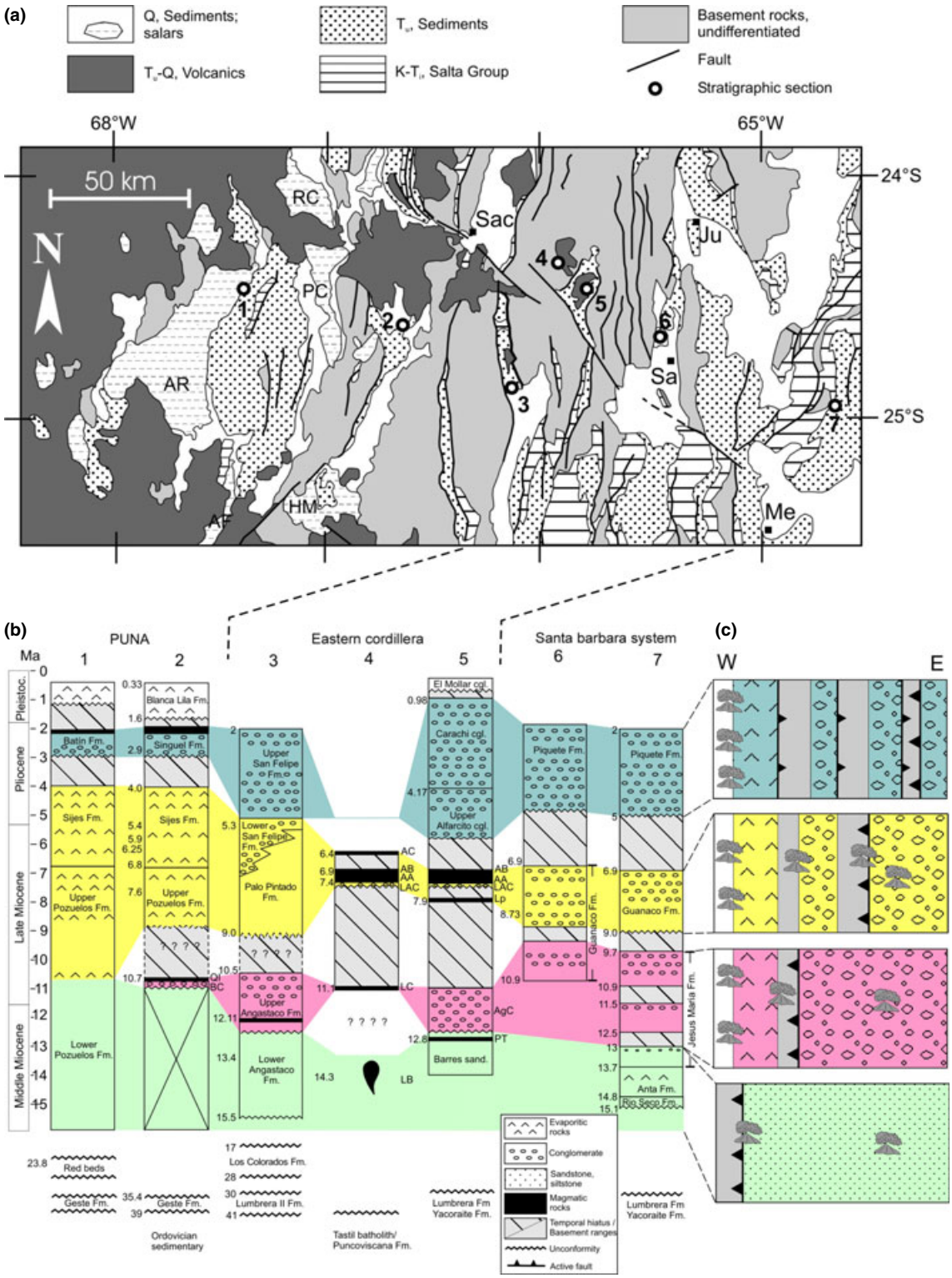

Fig. 11. Regional distribution (a; location as in Fig. 1c) and correlation (b) among middle Miocene–Pliocene deposits along a transect at *ca.* 24° S from western Puna to Santa Barbara System. Location, lithology and age (on the left side of logs) of stratigraphic sections are based on the following: (1) Salar de Arizaro (Donato,1987; Coutand *et al.*, 2001); (2) Salar de Pastos Grandes (Alonso, 1992; DeCelles *et al.*, 2007); (3) Calchaquí Valley (Carrera & Muñoz, 2008); (4) Almagro range (this paper); (5) El Toro basin (Marrett & Strecker, 2000; Mazzuoli *et al.*, 2008; this paper); (6) Rio Yacones (Viramonte *et al.*, 1994); (7) Arroyo Gonzalez (Reynolds *et al.*, 2000). The middle Miocene–Pliocene stratigraphy is divided into four sequences indicated by differently coloured bands. See the text for discussion. AA, Almagro A member; AB, Almagro B member; AC, Almagro C member; AgC, Agujas conglomerate; BC, black conglomerate; LAC, Lower Alfarcito conglomerate; LB, Las Burras member; LC, Las Cuevas member; Lp, Lampazar member; QI, Quevar Ignimbrite; PT, Puerta Tastil member. (c) Schematic reconstruction of paleogeography and magmatic activity coeval with the proposed depositional sequences. Not to scale. Colours as in Fig. 11b.

stratigraphy of the Eastern Cordillera and Santa Barbara System can be divided into four sequences (see also Starck & Anzótegui, 2001; Carrera & Muñoz, 2008). The basal sequence (*ca*. 15–12.5 Ma) is dominated by fine-grained deposits representing eolian sandstones (lower member of Angastaco and Rio Seco Formations; Reynolds *et al.*, 2000; Coutand *et al.*, 2006; Carrera & Muñoz, 2008), sandy distal alluvial plains (Barres sandstone and lower member of Jesus Maria Formation; Marrett & Strecker, 2000; Reynolds *et al.*, 2000; this article) and playa-lake gypsum and limestone (Anta Formation; Galli *et al.*, 1996; Reynolds *et al.*, 2000; Fig. 11b). Subsequently, an abrupt eastward progradation of fluvial and alluvial conglomerates occurred between 12.5 and 9.7 Ma (upper member of Angastaco Formation, Agujas conglomerate and upper member of Jesus Maria Formation; Marrett & Strecker, 2000; Reynolds *et al.*, 2000; Coutand *et al.*, 2006; Carrera & Muñoz, 2008; this article). A gap in sedimentation, lasting up to 4 Ma in the Almagro–El Toro basin, probably has regional extent (Alonso, 2000; Reynolds *et al.*, 2000; Carrera & Muñoz, 2008; Fig. 11b).

During the third sequence (9–6.9 Ma), the foreland system experienced different along-strike patterns of deformation and sediment accumulation. S of 25° S, a contiguous depositional system was defined across the foreland, from the western Eastern Cordillera (Palo Pintado Formation) to the Santa Barbara System (Guanaco Formation) (Hain *et al.*, 2011). In the studied transect at 24° S, the continuity of the foreland basin was partitioned by the deformation and uplift of the Almagro–El Toro area, as suggested by frequent hiatuses, unconformities and growth strata. In particular, in the W, the deposition of conglomerates continued in alluvial fans situated at the orogenic front (lower member of San Felipe Formation) and prograded eastward into fine-grained sediments of a floodplain with ponds and swamps (Palo Pintado Formation; Coutand *et al.*, 2006; Carrera & Muñoz, 2008; Fig. 11b). In the stratigraphic section of the Almagro–El Toro area, the sedimentation was dominated by back-arc magmatism (BAT members) and localised alluvial fans (lower Alfarcito conglomerate). Eastwards, alluvial fans and braided streams shed conglomerates and sandstones of the Guanaco Formation (Viramonte *et al.*, 1994; Reynolds *et al.*, 2000; Fig. 11b).

Finally, during Pliocene, the deposition of coarse conglomerates of alluvial fans (upper member of San Felipe Formation, upper Alfarcito and Carachi conglomerates, Piquete Formation; Viramonte *et al.*, 1994; Marrett & Strecker, 2000; Reynolds *et al.*, 2000; Carrera & Muñoz, 2008; Fig. 11b) was restricted to intermontane depocentres and fed by bounding ranges of the compartmentalised foreland basin system.

A tectono-sedimentary model

We point to two major questions concerning the Cenozoic evolution of the central Andean foreland: (1) the timing of onset of Andean orogenic shortening and its kinematic history and (2) the style and progression of orogenic deformation and uplift affecting the Andean foreland basin.

(1) In the Almagro–El Toro basin, at 24°30′ S, major compressive phases occur between 12.5 and 11.1 Ma. The exposure of the Neoproterozoic–Lower Cambrian crystalline basement prior to the emplacement of the Las Cuevas volcanics at 11.1 Ma indicates the minimum age of significant rock uplift and erosion in this part of the Eastern Cordillera. The age of this shortening event is consistent with the age proposed for the paleogeographic isolation of the Puna plateau (Vandervoort *et al.*, 1995). The tectonically active front propagated eastward in the medial part of the El Toro basin from *ca*. 7.9 Ma (Fig. 10). Minor renewed deformation occurred at 7.9–7.5 Ma, <7.5 and <7.2 Ma during episodic volcanism. Main surface uplift occurred likely after 6.4 Ma.

This episodic compression, alternated with relative quiescence, may be related to magmatic activity, the thick-skinned structure, the interference with the transverse COT fault zone and the inherited pre-Andean features. In particular, the second phase of BAT magmatism, starting at 11.1 Ma, has an isotopic composition indicative of an anomalously enriched mantle source that was interpreted as a consequence of lithospheric delamination and asthenospheric upward flux (Mazzuoli *et al.*, 2008). The uprise of asthenosphere may have (1) triggered the major foreland deformation and rapid Eastern Cordillera exhumation and erosion recorded between 12.5 and 11.1 Ma (Fig. 10f), and (2) produced a thermal weakening within the crust.

(2) The along-strike differences of the depositional and structural evolution (Kley, 1996; Kley *et al.*, 1999) support two models concerning the Cenozoic evolution and progression of the shortening of the Central Andean foreland. The first model proposes a systematic eastward propagation of the deformation front, with an integrated foreland basin system migrating from the Western Cordillera to the Chaco basin since the Cretaceous (Noblet *et al.*, 1996; Horton, 1998; Reynolds *et al.*, 2000; Coutand *et al.*, 2001; DeCelles & Horton, 2003; Kley *et al.*, 2005). This sequential eastward migration is applied mainly to the thin-skinned fold-and-thrust belt of northern Eastern Cordillera and Sierras Subandinas (DeCelles & Horton, 1999, 2003; Horton *et al.*, 2001; Siks & Horton, 2011). The alternative model suggests an irregular and disorganised progression of deformation creating fragmented intermontane basins (Alonso *et al.*, 2006; Hongn *et al.*, 2007; Mortimer *et al.*, 2007; Bosio *et al.*, 2009). This broken foreland model has been applied to the thick-skinned structure of the southern Eastern Cordillera, Santa Barbara System and Sierras Pampeanas. In particular, in the Eastern Cordillera, S of 25° S, basement-cored ranges and intervening intermontane basins are interpreted as the result of the spatially and temporally disparate Neogene contractile inversion of the normal faults of Cretaceous Salta Rift (Grier *et al.*, 1991; Kley & Monaldi,

2002; Carrera *et al.*, 2006; Carrera & Muñoz, 2008; Hain *et al.*, 2011).

The stratigraphic, sedimentologic and structural data presented in this article provide some constraints on the middle-late Miocene foreland evolution. (a) From the Puna border to the Sierra de Pasha, the Salta Group strata are represented by marine (Yacoraite Formation) and non-marine (red beds) deposits (late Campanian–middle Eocene) pertaining to a single integrated basin without evidence of the synrift deposits and tectonics of the Salta Rift (Figs 1 and 2). (b) The middle-upper Miocene stratigraphy records an overall upward coarsening from the fine-grained lower portion to the final deposition of very coarse conglomerate facies with extreme textural and compositional immaturity. (c) The compressional tectonic structure is interpreted as a series of fault-propagation folds (San Bernardo Fault and intrabasinal folds) with various types of growth structures (Figs 2 and 10). The synorogenic conglomerates progressively rest in angular unconformity upon the folded rocks associated with these faults (Fig. 10). (d) The absence of significant intrabasinal tectonic structures in the lower part and the presence of several local and regional unconformities in the upper part of the foreland deposits record the temporal and spatial eastward and up-section progression of the deformation.

Based on these observations, we propose that the sequential eastward (forelandward) progression of deformation is the more plausible foreland model for the Almagro-El Toro region, although the crucial question concerning the presence of a basal decollement accommodating the foreland shortening remains unanswered. The lower part of the sequence (Barres sandstone) can be related to a distal depozone characterised by a broad, flat and low-energy alluvial environment. The thick and coarse-grained deposits of the medial part (Agujas conglomerate) suggest the onset of uplift and exhumation of the western Eastern Cordillera. The upper part of the sequence (from Las Cuevas to Almagro B members) accumulated on top of the buried growing structures of the frontal part of the orogenic wedge, recording its syndepositional deformation between 11.1 and 6.4 Ma (Fig. 10).

CONCLUSIONS

(1) The middle-upper Miocene Almagro-El Toro non-marine volcano-sedimentary sequence consists of the following: (a) a lower interval (14.3–12.5 Ma) of red floodplain sandstones and siltstones developed at the expense of the Cretaceous-Paleogene Salta Group strata that were uplifted and unroofed in the incipient deformation of the W part of the Eastern Cordillera, (b) a medial interval (12.5–7.5 Ma) of non-volcanogenic conglomerates with localised volcanic centres showing synvolcanic and syndepositional folding and faulting and (c) an upper interval (7.5–6.9 Ma) of volcanogenic coarse conglomerates and breccia that partly buried the orogenic wedge front. The most abundant lithofacies is disorganised, matrix-supported, pebble-boulder conglomerate showing planar bedding over lateral distances of tens to hundreds of metres. This predominant lithofacies is irrespective of any volcanogenic or non-volcanogenic composition of the conglomerate clasts, suggesting a consistent mechanism and environment of deposition. Overall, the general coarsening-upward trend, geometry of beds, coarse grain-size and distribution of lithofacies are attributed to an eastward progradation of sediment gravity flow-dominated (debris-flow and sheet flow) alluvial fan systems without sizeable fluvial system rivers in a context of low topographic relief.

(2) During the middle-late Miocene, the Almagro-El Toro basin was an integral part of the Central Andean foreland basin, extending as a continuous depositional system until 6.4 Ma (Fig. 10). The upward transition from fine-grained undeformed distal alluvial plain (Barres sandstone) to coarse-grained alluvial fan (Agujas conglomerate) and to growth strata of localised depocentres and volcanism (Las Cuevas, Lampazar and lower Alfarcito conglomerate) marks the evolution of the basin from a distal foreland basin to a wedge-top depozone. This defines the time at which the frontal orogenic belt propagated eastwards.

(3) The Almagro-El Toro sequence experienced several deformation episodes concomitantly with the development of the Eastern Cordillera thrust-fold belt and can be considered an evolving wedge-top depozone that was active since at least 11.1 Ma. Reconstruction of unroofing shows uplift and exhumation of *ca.* 6.5 km of section (Fig. 10f). The conglomerate clast composition records the unroofing of western sources (the eastern margin of Puna and western Eastern Cordillera). The Almagro-El Toro sediments blanked the active thrust front (the E-verging San Bernardo fault-propagation fold), and advance of its related blind thrusts and folds deformed the foreland basin sequence by intrabasinal faulting and folding.

(4) We contribute to determining the onset of shortening and exhumation of the southern Eastern Cordillera. Between 14.3 and 6.4 Ma, the foreland basin system of Central Andes at 24°30′ S experienced eight major tectonically driven syndepositional events and six volcanic episodes; the latter is related to the activity of the N-striking faults of the Eastern Cordillera and to NW-striking COT faults. The sedimentation of the Barres sandstone as a result of the erosion of Salta Group strata and the emplacement of the Las Burras laccolith may be related to an early stage of deformation and exhumation at *ca.* 14–12.5 Ma, masked by the non-resistant lithologies of the source region. Major compression occurred between 12.5 and 11.1 Ma, exhumating and unroofing the area between the eastern margin of Puna plateau and the Almagro range that was stripped of its Neoproterozoic-

Paleozoic cover, coeval with the deposition of a debris flow-dominated alluvial-fan system.

ACKNOWLEDGEMENTS

This work was carried out with the financial support of Italian Ministry of University and Research (MIUR-PRIN 2003 project), and in the framework of the scientific convention between Pisa and Salta Universities (Projects PID CONICET Nº 5341 and CIUNSA 20/D-249, Salta University, Argentina). We thank Massimo Matteini and Andrea Uttini for assistance during the fieldwork. We also thank the editor B.K. Horton, I. Petrinovic and an anonymous reviewer for their thorough comments and suggestions that greatly improved the quality of our work.

SUPPORTING INFORMATION

Additional Supporting Information may be found in the online version of this article:

Figure S1. (A) The stratigraphic transect at the head of the quebrada Carachi (Section 3 in Fig. 2) shows Barres sandstone and interbedded lavas of Puerta Tastil member (K/Ar age of 12.78 ± 0.19 Ma; Mazzuoli *et al.*, 2008) folded in a NNE-plunging anticline. (B) At the mouth of the quebrada Lagunillas (Section 8 in Fig. 2), contact between the Puncoviscana Formation (PV) and lower Alfarcito conglomerate (LAC) is both stratigraphic (onlapping) (white line) and tectonic (red line) along a NW-striking fault zone. The subvertical fault planes are oblique with respect to the E-W-oriented outcrop front and have N120° E strike and N30° E dip direction. The basement-derived massive conglomerate (Gmm/cm) with interbedded sandstone (Sm/h) of the lower Alfarcito conglomerate shows syntectonic growth structures.

Figure S2. Overviews of the stratigraphic and tectonic relations between the granodiorite of the Santa Rosa de Tastil batholith (STR), Las Cuevas member (LC) and lower Alfarcito conglomerate (LAC), to the N (A) and SW (B) of Alfarcito village (Section 1 in Fig. 2). Contacts are either stratigraphic overlapping (dashed lines) or faults (solid lines). The San Bernardo fault thrusts the Santa Rosa de Tastil grey granodiorite over the Miocene volcano-sedimentary deposits of the El Toro basin. Syn-sedimentary faults deform contacts among the Las Cuevas member, lower Alfarcito conglomerate and granodiorite. The unconformity between the Las Cuevas member and the lower Alfarcito conglomerate represents a hiatus of *ca.* 4 Ma.

Figure S3. The stratigraphic transect measured at quebrada Carachi (Section 2 in Fig. 2). (A) Detail of the paraconcordant contact between the lower Alfarcito conglomerate (LAC) and Almagro A member (AA; RGcm facies). (B) Unconformable (15°) and erosive contact between the Almagro A member and lower Alfarcito conglomerate. A boulder conglomerate facies (RGcm) is at the edge of the channel-like incision; sub-horizontally stratified sandstone and mudstone facies (Vsh) aggraded into the channel; a boulder conglomerate facies (VGmm/cm) levels the sequence. The red box is Fig. S3C. (C) Detail (arrow) of flame structures on lacustrine laminated mudstones squeezed upward for the load of overlying conglomerate near the base of the Almagro A member. Hammer is 30 cm long. Representative conglomerate facies of the Almagro A member (Section 4; Fig. 3). Hammer is 30 cm long. (D) Close-up view of a clast of fresh, vesiculated lava showing jigsaw fractures (arrows) infilled by fine-sandy matrix (RGcm facies). (E) Clast-supported, polygenetic pebble–cobble conglomerate facies (VGmm/cm facies).

Figure S4. Representative conglomerate facies of the Almagro B member. (A) Lower layer is a debris-flow deposit comprising matrix-supported conglomerate (VGmm/cm facies) with subvertical degassing pipes (arrows). Upper bed is a clast-supported coarse breccia from syneruptive debris avalanche (RBcm/mm facies) with basal erosive surface. Exposure is 6 m thick (Section 9). (B) Overview of stacked debris-flow beds (VGmm/cm facies; Section 9). Cobble-boulder conglomerate is matrix- to clast-supported, poorly sorted and with non-homogeneous concentration of clasts. Individual conglomerate clasts are angular to subangular, indicating minimal reworking prior to deposition. Rule is 1 m long. (C) A very coarse, clast-supported, polygenetic boulder conglomerate (VGcm) is at the base of the Almagro B member (Section 4; Fig. 3).

Please note: Wiley-Blackwell are not responsible for the content or functionality of any supporting materials supplied by the authors. Any queries (other than missing material) should be directed to the corresponding author for the article.

REFERENCES

Acocella, V., Vezzoli, L., Omarini, R., Matteini, M. & Mazzuoli, R. (2007) Kinematic variations across Eastern Cordillera at 24°S (Central Andes): tectonic and magmatic implications. *Tectonophysics*, **434**, 81–92, doi: 10.1016/j.tecto.2007.02.001.

Acocella, V., Gioncada, A., Omarini, R., Riller, U., Mazzuoli, R. & Vezzoli, L. (2011) Tectonomagmatic characteristics of the back-arc portion of the Calama-Olacapato-El Toro Fault Zone, Central Andes. *Tectonics*, **30**, TC3005, doi: 10.1029/2010TC002854.

Allmendinger, R.W., Ramos, V., Jordan, T., Palma, M. & Isacks, B.L. (1983) Paleogeography and Andean structural geometry, Northwestern Argentina. *Tectonics*, **2**, 1–16.

Allmendinger, R.W., Jordan, T.E., Kay, S.M. & Isacks, B.L. (1997) The evolution of the Altiplano-Puna Plateau of the Central Andes. *Annual Rev. Earth Planet. Sci.*, **25**, 139–174.

Alonso, R.N. (1992) Estratigrafia del Cenozoico de la cuenca de Pastos Grandes (Puna Salteña) con énfasis en la Formación Sijes y sus boratos. *Rev. Asoc. Geol. Arg.*, **47**, 189–199.

Alonso, R.N. (2000) El Terciario de la Puna en tiempos de la ingresión marina parananse. In: *El Neógeno de Argentina* (Ed. by F.G. Aceñolaza & T. Herbst) *Serie Correlación Geológica*, **14**, 1663–1680.

Alonso, R.N., Carrapa, B., Coutand, I., Haschke, M., Hilley, G.E., Schoenbohm, L., Sobel, E.R., Strecker, M. R. & Trauth, M.H. (2006) Tectonics, climate, and landscape evolution of the southern Central Andes: the Argentine Puna Plateau and adjacent Regions between 22º and 28ºS lat. In: *The Andes – Active Subduction Orogeny* (Ed. by O. Oncken, G. Chong, G. Franz, P. Giese, H.-J. Götze, V.A. Ramos, M.R. Strecker & P. Wigger), pp. 265–283. Springer Verlag, Berlin, NY.

Andriessen, P.A.M. & Reutter, K.-J. (1994) K-Ar and fission-track mineral age determination of igneous rocks related to multiple magmatic arc systems along the 23°S latitude of Chile and NW Argentina. In: *Tectonics of the Southern Central Andes* (Ed. by K.-J. Reutter, E. Scheuber & P. Wigger), pp. 141–153. Springer Verlag, Berlin, NY.

Barazangi, M. & Isacks, B.L. (1976) Spatial distribution of earthquakes and subduction of the Nazca Plate beneath South America. *Geology*, **4**, 686–692.

Beck, R.A., Vondra, C.F., Filkins, J.E. & Olander, J.D. (1988) Syntectonic sedimentation and Laramide basement thrusting, Cordilleran foreland; timing of deformation. In: *Interaction of the Rocky Mountain foreland and the Cordilleran thrust belt* (Ed. by C.J. Schmidt & W.J. Perry, Jr.) *Geol. Soc. Am. Memoir*, **171**, 465–487.

Blair, T.C. (1999) Sedimentology of the debris-flow-dominated Warm Spring Canyon alluvial fan, Death Valley, California. *Sedimentology*, **46**, 941–965.

Blair, T.C. & McPherson, J.G. (1994) Alluvial fans and their natural distinction from rivers based on morphology, hydraulic processes, sedimentary processes, and facies assemblages. *J. Sedimentary Res.*, **64**, 450–489.

Blasco, G., Zappettini, E.O. & Hongn, F. (1996) Hoja geológica 2566-1, San Antonio de los Cobres, *Programa Nacional de carteas Geológicas de la República Argentina*. Dir. Nac. del Servicio geológico. Buenos Aires, Argentina.

Bosio, P.P., Powell, J., Del Papa, C. & Hongn, F. (2009) Middle Eocene deformation–sedimentation in the Luracatao Valley: tracking the beginning of the foreland basin of northwestern Argentina. *J. South Am. Earth Sci.*, **28**, 142–154, doi: 10.1016/j.jsames.2009.06.002.

Bossi, G.E., Georgieff, S.M., Gavriloff, I.J.C., Ibañez, L.M. & Muruaga, C.M. (2001) Cenozoic evolution of the intramontane Santa María basin, Pampean Ranges, northwestern Argentina. *J. South Am. Earth Sci.*, **14**, 725–734.

Burbank, D.W., Puigdefabregas, C. & Muñoz, J.A. (1992) The chronology of the Eocene tectonic and stratigraphic development of the eastern Pyrenean foreland basin, northeast Spain. *Geol. Soc. Am. Bull.*, **104**, 1101–1120.

Carrera, N. & Muñoz, J.A. (2008) Thrusting evolution in the southern Cordillera Oriental (northern Argentine Andes): constraints from growth strata. *Tectonophysics*, **459**, 107–122.

Carrera, N., Munoz, J.A., Sabat, F., Mon, R. & Roca, E. (2006) The role of inversion tectonics in the structure of the Cordillera Oriental (NW Argentina Andes). *J. Struc. Geol.*, **28**, 1921–1932.

Coira, B., Kay, S.M. & Viramonte, J. (1993) Upper Cenozoic magmatic evolution of the Argentine Puna – A model for changing subduction geometry. *Int. Geol. Review*, **35**, 677–720.

Coutand, I., Cobbold, P.R., De Urreiztieta, M., Gautier, P., Chauvin, A., Gapais, D., Rossello, E.A. & Lopez-Gamundi, O. (2001) Style and history of Andean deformation, Puna plateau, northwestern Argentina. *Tectonics*, **20**, 210–234.

Coutand, I., Carrapa, B., Deeken, A., Schmitt, A.K., Sobel, E.R. & Strecker, M.R. (2006) Propagation of orographic barriers along an active range front: insights from sandstone petrography and detrital apatite fission-track thermochronology in the intramontane Angastaco basin, NW Argentina. *Basin Res.*, **18**, 1–26.

Davila, F.M. & Astini, R.A. (2007) Cenozoic provenance history of synorogenic conglomerates in western Argentina (Famatina belt): implications for Central Andes foreland development. *Geol. Soc. Am. Bull.*, **119**, 609–622.

DeCelles, P.G. & Horton, B.K. (1999) Implications of early Tertiary foreland basin development for orogenesis in the central Andes. *Eos*, **80**, 1052.

DeCelles, P.G. & Horton, B.K. (2003) Early to middle Tertiary foreland basin development and the history of Andean crustal shortening in Bolivia. *Geol. Soc. Am. Bull.*, **115**, 58–77.

DeCelles, P.G., Gray, M.B., Ridgway, K.D., Cole, R.B., Srivastava, P., Pequera, N. & Pivnik, D.A. (1991) Kinematic history of a foreland uplift from Paleocene synorogenic conglomerate, Beartooth Range, Wyoming and Montana. *Geol. Soc. Am. Bull.*, **103**, 1458–1475.

DeCelles, P.G., Pile, H.T. & Coogan, J.C. (1993) Kinematic history of the Meade thrust based on provenance of the Bechler conglomerate at Red Mountain, Idaho, Sevier thrust belt. *Tectonics*, **12**, 1436–1450.

DeCelles, P.G., Gehrels, G.E., Quade, J., Ojha, T.P., Kapp, P.A. & Upreti, B.N. (1998) Neogene foreland basin deposits, erosional unroofing, and the kinematic history of the Himalayan fold-thrust belt, western Nepal. *Geol. Soc. Am. Bull.*, **110**, 2–21.

DeCelles, P.G., Carrapa, B. & Gehrels, G.E. (2007) Detrital zircon U-Pb ages provide provenance and chronostratigraphic information from Eocene synorogenic deposits in northwestern Argentina. *Geology*, **35**, 323–326, doi: 10.1130/G23322A.1

Deeken, A., Sobel, E.R., Coutand, I., Haschke, M., Riller, U. & Strecker, M.R. (2006) Development of the southern Eastern Cordillera, NW Argentina, constrained by apatite fission track thermochronology: from Early Cretaceous extension to middle Miocene shortening. *Tectonics*, **25**, TC6003, doi: 10.1029/2005TC001894.

Donato, E. (1987) Caracteristicas estructurales del sector occidental de la Puna Salteña. *Bol. Information Petrolera*, **12**, 89–97.

Fossen, H. & Tikoff, B. (1998) Extended models of transpression and transtension, and application to tectonic settings. In: *Continental Transpressional and Transtensional Tectonics* (Ed. by R.E. Holdsworth, R.A. Strachan & J.F. Dewey) *Geol. Soc. Spec. Publ.*, **135**, 15–33.

Galli, C.I., Hernandéz, R.M. & Reynolds, J.H. (1996) Análisis paleoambiental y ubicacíon geocronológica del Subgruppo Metán: Salta, Argentina. *Bol. Information Petrolera*, **12**, 99–107.

Gebhard, J.A., Giudice, A.R. & Gascon, J.O. (1974) Geologia de la comarca entre el Rio Juramento y Arroyo las Tortugas, provincias de Salta y Jujuy, Republica Argentina. *Rev. Ass. Geol. Arg.*, **29**, 359–375.

Gioncada, A., Vezzoli, L., Mazzuoli, R., Omarini, R., Nonnotte, P. & Guillou, H. (2010) Pliocene intraplate-type volcanism in the Andean foreland at 26°10′S, 64°40′W (NW Argentina): implications for magmatic and structural evolution of the Central Andes. *Lithosphere*, **2**, 153–171, doi: 10.1130/L81.1.

Graham, S.A., Tolson, R.B., DeCelles, P.G., Ingersoll, R. V., Bargar, E., Caldwell, M., Cavazza, W., Edwards, D. P., Follo, M.F., Handschy, J.W., Lemke, L., Moxon, I., Rice, R., Smith, G.A. & White, J. (1986) Provenance modelling as a technique for analysing source terrane evolution and controls of foreland sedimentation. In: *Foreland Basins* (Ed. by P.A. Allen & P. Homewood) *Spec. Publ. Int. Ass. Sediment.*, **8**, 425–436.

Grier, M.E., Salfity, J.A. & Allmendinger, R.W. (1991) Andean reactivation of the Cretaceous Salta rift, northwestern Argentina. *J. South Am. Earth Sci.*, **4**, 351–372.

Hain, M.P., Strecker, M.R., Bookhagen, B., Alonso, R.N., Pingel, H. & Schmitt, A.K. (2011) Neogene to Quaternary broken foreland formation and sedimentation dynamics in the Andes of NW Argentina (25°S). *Tectonics*, **30**, TC2006, doi: 10.1029/2010TC002703.

Hampton, B.A. & Horton, B.K. (2007) Sheetflow fluvial processes in a rapidly subsiding basin, Altiplano plateau, Bolivia. *Sedimentology*, **54**, 1121–1147.

Hardy, S. & Poblet, J. (1994) Geometric and numerical model of progressive limb rotation in detachment folds. *Geology*, **22**, 371–374.

Hendrix, M.S., Graham, S.A., Carroll, A.R., Sobel, E.R., Mcknight, C.L., Schulein, B.J. & Wang, Z. (1992) Sedimentary record and climatic implications of recurrent deformation in the Tian Shan: evidence from Mesozoic strata of the north Tarim, south Junggar, and Turpan basins, northwest China. *Geol. Soc. Am. Bull.*, **104**, 53–79.

Hernandéz, R.M., Galli, C.I. & Reynolds, J.H. (1999) Estratigrafia del Terciario en el Noroeste Argentino. In: *Geología del Noroeste Argentino* (Ed. by G. Gonzalez Bonorino, R. Omarini & G. Viramonte) *Relatorio XIV Congreso Geológico Argentino*, tomo **1**, 316–328.

Hilley, G.E. & Strecker, M.R. (2005) Processes of oscillatory basin filling and excavation in a tectonically active orogen: quebrada del Toro Basin, NW Argentina: *Geol. Soc. Am. Bull.*, **117**, 887–901.

Hongn, F., Del Papa, C., Powell, J., Petrinovic, I., Mon, R. & Deraco, V. (2007) Middle Eocene deformation and sedimentation in the Puna–Eastern Cordillera transition (23°–26° S): control by pre-existing heterogeneities on the pattern of initial Andean shortening. *Geology*, **35**, 271–274.

Hongn, F.D., Tubia, J.M., Aranguren, A., Vegas, N., Mon, R. & Dunning, G.R. (2010) Magmatism coeval with lower Paleozoic shelf basins in NW-Argentina (Tastil batholith): constraints on current stratigraphic and tectonic interpretations. *J. South Am. Earth Sci.*, **29**, 289–305.

Horton, B.K. (1998) Sediment accumulation on top of the Andean orogenic wedge: Oligocene to late Miocene basins of the eastern Cordillera, southern Bolivia. *Geol. Soc. Am. Bull.*, **110**, 1174–1192.

Horton, B.K. (2005) Revised deformation history of the central Andes: inferences from Cenozoic foredeep a intermontane basins of the Eastern Cordillera, Bolivia. *Tectonics*, **24**, TC3011, doi: 10.1029/2003TC001619.

Horton, B.K. & DeCelles, P.G. (1997) The modern foreland basin system adjacent to the Central Andes. *Geology*, **25**, 895–898.

Horton, B.K., Hampton, B.A. & Waanders, G.L. (2001) Paleogene synorogenic sedimentation in the Altiplano plateau and implications for initial mountain building in the central Andes. *Geol. Soc. Am. Bull.*, **113**, 1387–1400.

Horton, B.K., Hampton, B.A., La Reau, B.N. & Baldellon, E. (2002) Tertiary provenance history of the northern and central Altiplano Plateau (central Andean Bolivia): a detrital record of plateau-margins tectonics. *J. Sedimentary Res.*, **72**, 711–726.

Hubert, J.F. & Filipov, A.J. (1989) Debris-flow deposits in alluvial-fan on the west flank of the White Mountains, Owens Valley, California, USA. *Sed. Geol.*, **61**, 177–205.

Hubert, J.F. & Hyde, M.G. (1982) Sheet-flow deposits of graded beds and mudstones on an alluvial sand flat-playa system: upper Triassic Blomidan red beds, St. Mary's Bay, Nova Scotia. *Sedimentology*, **29**, 457–474.

Iaffa, D.N., Sàbat, F., Bello, D., Ferrer, O., Mon, R. & Gutierrez, A.A. (2011) Tectonic inversion in a segmented foreland basin from extensional to piggy back settings: the Tucumán basin in NW Argentina. *J. South Am. Earth Sci.*, **31**, 457–474.

Isacks, B.L. (1988) Uplift of the Central Andean plateau and bending of the Bolivian orocline. *J. Geophys. Res.*, **93**, 3211–3231.

Jordan, T.E. & Alonso, R.N. (1987) Cenozoic stratigraphy and basin tectonics of the Andes mountains, 20°–28° South Latitude. *Am. Ass. Petrol. Geol. Bull.*, **71**, 49–64.

Jordan, T.E., Isacks, B.L., Allmendinger, R.W., Brewer, J. A., Ramos, V.A. & Ando, C.J. (1983) Andean tectonics related to geometry of subducted Nazca plate. *Geol. Soc. Am. Bull.*, **94**, 341–361.

Jordan, T.E., Reynolds, J.H. & Erikson, P.J. (1997) Variability in age of initial shortening and uplift in the central Andes, 16-33°30′S. In: *Tectonic Uplift and Climate Change* (Ed. by W.F. Ruddiman), pp. 41–61. Plenum, New York.

Kilmurray, J.O. & Igarzabal, A.P. (1971) Petrografia y rasgos geomorficos del batolito granitico de Santa Rosa de Tastil, provincia de Salta, Rep. Argentina. *Rev. As. Geol. Arg.*, **26**, 417–438.

Kleinert, K. & Strecker, M.R. (2001) Climate change in response to orographic barrier uplift: paleosol and stable isotope evidence from the late Neogene Santa Maria basin, northwestern Argentina. *Geol. Soc. Am. Bull.*, **113**, 728–742.

Kley, J. (1996) Transition from basement-involved to thin-skinned thrusting of the Cordillera Oriental of southern Bolivia. *Tectonics*, **15**, 763–775.

Kley, J. & Monaldi, C.R. (2002) Tectonic inversion in the Santa Barbara System of the central Andean foreland thrust belt, northwestern Argentina. *Tectonics*, **21**, 1111–1118.

Kley, J., Gangui, A.H. & Krüger, D. (1996) Basement-involved blind thrusting in the eastern Cordillera Oriental, southern Bolivia: evidence from cross-sectional balancing, gravimetric and magnetotelluric data. *Tectonophysics*, **259**, 171–184.

Kley, J., Muller, J., Tawackoli, S., Jacobshagen, V. & Manutsoglu, E. (1997) Pre-Andean and Andean-age

deformation in the Eastern Cordillera of southern Bolivia. *J. South Am. Earth Sci.*, **10**, 1–19.

Kley, J., Monaldi, C.R. & Salfity, J.A. (1999) Along-strike segmentation of the Andean foreland: causes and consequences. *Tectonophysics*, **301**, 75–94.

Kley, J., Rossello, E.A., Monaldi, C.R. & Habighorst, B. (2005) Seismic and field evidence for selective inversion of Cretaceous normal faults, Salta rift, northwest Argentina. *Tectonophysics*, **399**, 155–172.

Marquillas, R.A. & Salfity, J.A. (1988) Tectonic framework and correlations of the Cretaceous-Eocene Salta Group; Argentina. *Lect. Notes Earth Sci.*, **17**, 119–136.

Marquillas, R.A., Del Papa, C. & Sabino, I.F. (2005) Sedimentary aspects and paleoenvironmental evolution of a rift basin: Salta Group (Cretaceous-Paleogene), northwestern Argentina. *Int. J. Earth Sci.*, **94**, 94–113.

Marrett, R. & Strecker, M.R. (2000) Response of intracontinental deformation in the central Andes to late Cenozoic reorganization of South American Plate motions. *Tectonics*, **19**, 452–467.

Marrett, R.A., Allmendinger, R.W., Alonso, R.N. & Drake, R.E. (1994) Late Cenozoic tectonic evolution of the Puna plateau and adjacent foreland, northwestern Argentine Andes. *J. South Am. Earth Sci.*, **7**, 179–207.

Matteini, M., Mazzuoli, R., Omarini, R., Cas, R. & Maas, R. (2002) Geodynamical evolution of the central Andes at 24°S as inferred by magma composition along the Calama-Olacapato-El Toro transversal volcanic belt. *J. Volcanol. Geotherm. Res.*, **118**, 225–228.

Mazzuoli, R., Vezzoli, L., Omarini, R., Acocella, V., Gioncada, A., Matteini, M., Dini, A., Guillou, H., Hauser, N., Uttini, A. & Scaillet, S. (2008) Miocene magmatism and tectonics in the easternmost sector of the Calama-Olacapato-El Toro fault system in Central Andes at ~24°S: Insights into the evolution of the Eastern Cordillera. *Geol. Soc. Am. Bull.*, **120**, 1493–1517.

McPhie, J., Doyle, M. & Allen, R. (1993) *Volcanic Textures: A Guide to the Interpretation of Textures in Volcanic Rocks*. Centre for Ore Deposit and Exploration Studies University of Tasmania, Hobart, Australia, 198 pp.

Miall, A.D. (1978) Lithofacies type and vertical profile models in braided river deposits: a summary. In: *Fluvial Sedimentology* (Ed. by A.D. Miall) *Can. Soc. Petrol. Geol. Memoirs*, **5**, 597–604.

Mon, R. (1999) Cordillera Oriental. In: *Geología del Noroeste Argentino* (Ed. by G. Gonzalez Bonorino, R. Omarini & G. Viramonte) *Relatorio XIV Congreso Geológico Argentino*, tomo **1**, 426–431.

Mortimer, E., Carrapa, B., Coutand, I., Schoenbohm, L., Sobel, E.R., Sosa Gomez, J. & Strecker, M.R. (2007) Fragmentation of a foreland basin in response to out-of-sequence basement uplifts and structural reactivation: El Cajon-Campo del Arenal basin, NW Argentina. *Geol. Soc. Am. Bull.*, **119**, 637–653.

Moya, M.C. (1999) El Ordovícico de los Andes del Norte Argentino. In: *Geología del Noroeste Argentino* (Ed. by G. Gonzalez Bonorino, R. Omarini & G. Viramonte) *Relatorio XIV Congreso Geológico Argentino*, tomo **1**, 134–152.

Nemec, W. & Steel, R.J. (1984) Alluvial and coastal conglomerates: their significant features and some comments on gravelly mass-flow deposits. In: *Sedimentology of Gravel and Conglomerates* (Ed. by E.H. Koster & R.J. Steel) *Can. Soc. Petrol. Geol. Memoir*, **10**, 1–31.

Noblet, C., Lavenu, A. & Marocco, R. (1996) Concept of continuum as opposed to periodic tectonism in the Andes. *Tectonophysics*, **255**, 65–78, doi: 10.1016/0040-1951(95)00081-X.

Omarini, R.H., Sureda, R.J., Gotze, H.-J., Seilacher, A. & Pfluger, F. (1999) Puncoviscana folded belt in northwestern Argentina: testimony of Late Proteroizoic Rodinia fragmentation and pre-Gondwana collisional episodes. *Int. J. Earth Sci.*, **88**, 76–97.

Payrola Bosio, P., Powell, J., Del Papa, C. & Hongn, F. (2009) Middle Eocene deformation-sedimentation in the Luracatao Valley: Tracking the beginning of the foreland basin of north western Argentina. *J. South Am. Earth Sc.*, **28**, 142–154.

Petrinovic, I.A., Riller, U. & Brod, A. (2005) The Negra Muerta volcanic complex, Southern Central Andes: geochemical characteristics and magmatic evolution of an episodic volcanic centre. *J. Volcanol. Geotherm. Res.*, **140**, 295–320.

Petrinovic, I.A., Martí, J., Aguirre-Díaz, G.J., Guzmán, S., Geyer, A. & Salado Paz, N. (2010) The Cerro Aguas Calientes caldera, NW Argentina: an example of a tectonically controlled, polygenetic collapse caldera, and its regional significance. *J. Volcanol. Geotherm. Res.*, **194**, 15–26.

Pierson, T.C. (1980) Erosion and deposition by debris flows at Mt. Thomas, North Canterbury, New Zealand. *Earth Surf. Process.*, **5**, 227–247.

Pierson, T.C. & Costa, J.E. (1987) A rheologic classification of subaerial sediment-water flows. *Geol. Soc. Am. Reviews in Engin. Geol.*, **7**, 1–12.

Pierson, T.C. & Scott, K.M. (1985) Downstream dilution of a lahar: transition from debris flow to hyperconcentrated stream flow. *Water Resour. Res.*, **21**, 1511–1524.

Reynolds, J.H., Galli, C.J., Hernandez, R.M., Idleman, B. D., Kotila, J.M., Hilliard, R.V. & Naeser, C.W. (2000) Middle Miocene tectonic development of the Transition Zone, Salta Province, northwest Argentina: magnetic stratigraphy from the Metàn Subgroup, Sierra de Gonzalez. *Geol. Soc. Am. Bull.*, **112**, 1736–1751.

Riller, U., Petrinovic, I.A., Ramelow, J., Strecker, M.R. & Oncken, O. (2001) Late Cenozoic tectonism, collapse caldera and plateau formation in the Central Andes. *Earth Planet. Sci. Lett.*, **188**, 299–311.

Salvini, F. & Storti, F. (2002) Three-dimensional architecture of growth strata associated to fault-bend, fault-propagation, and décollement anticlines in non-erosional environments. *Sed. Geol.*, **146**, 57–73.

Sanchez, M.C. & Salfity, J.A. (1999) La cuenca cámbrica del Grupo Meson en el Noroeste Argentino: desarrollo estratigrafico y paleogeografico. *Acta Geol. Hispanica*, **34**, 123–139.

Schultz, A.W. (1984) Subaerial debris flow deposition in the Upper Paleozoic Cutler Formation, western Colorado. *J. Sed. Petrol.*, **54**, 759–772.

Schwab, K. & Schäfer, A. (1976) Sedimentation und Tektonik im mittleren abschnitt des Rio Toro in der Ostkordillere NW-Argentiniens. *Geol. Rundschau*, **65**, 175–194.

Siks, B.C. & Horton, B.K. (2011) Growth and fragmentation of the Andean foreland basin during eastward advance of fold-thrust deformation, Puna plateau and Eastern Cordillera, northern Argentina. *Tectonics*, **30**, TC6017, doi: 10.1029/2011TC002944, 2011

Smith, G.A. (1986) Coarse-grained nonmarine volcaniclastic sediment: terminology and depositional process. *Geol. Soc. Am. Bull.*, **97**, 1–10.

Smith, G.A. (1991) Facies sequences and geometries in continental volcaniclastic sediments. In: *Sedimentation in Volcanic Settings* (Ed. by R.V. Fisher & G.A. Smith) *SEPM Spec. Publ.*, **45**, 109–121.

Smith, G.A. & Lowe, D.R. (1991) Lahars: volcano-hydrologic events and deposition in the debris flow-hyperconcentrated flow continuum. In: *Sedimentation in Volcanic Settings* (Ed. by R.V. Fisher & G.A. Smith) *SEPM Spec. Publ.*, **45**, 59–70.

Sobel, E.R. & Strecker, M.R. (2003) Uplift, exhumation and precipitation: tectonic and climatic control of Late Cenozoic landscape evolution in the northern Sierras Pampeanas, Argentina. *Basin Res.*, **15**, 431–451, doi: 10.1046/j.1365-2117.2003.00214.x

Sobel, E.R., Hilley, G.E. & Strecker, M.W. (2003) Formation of the internally drained contractional basins by aridity-limited bedrock incisions. *J. Geophys. Res.*, **108**, 2344, doi: 10.1029.2002JB001883.

Spotila, J.A., Farley, K.A., Yule, J.D. & Reiners, P.W. (2001) Near-field transpressive deformation along the San Andreas fault zone in southern California, based on exhumation constrained by (U-Th)/He dating. *J. Geophys. Res.*, **106**, 30909–30922.

Starck, D. & Anzótegui, L.M. (2001) The late Miocene climate change – persistence of a climatic signal through the orogenic stratigraphic record in northwestern Argentina. *J. South Am. Earth Sci.*, **14**, 763–774.

Strecker, M.R., Cerveny, P., Bloom, A.L. & Malizia, D. (1989) Late Cenozoic tectonism and landscape development in the foreland of the Andes: Northern Sierras Pampeanas (26°–28°S), Argentina. *Tectonics*, **8**, 517–534.

Strecker, M.R., Alonso, R.N., Bookhagen, B., Carrapa, B., Coutand, I., Hain, M.P., Hilley, G.E., Mortimer, E., Schoenbohm, L. & Sobel, E.R. (2009) Does the topographic distribution of the central Andean Puna Plateau result from climatic or geodynamic processes? *Geology*, **37**, 643–646.

Sylvester, A.G. (1988) Strike-slip faults. *Geol. Soc. Am. Bull.*, **100**, 1666–1703.

Trauth, M.H. & Strecker, M.R. (1999) Formation of landslide-dammed lakes during a wet period between 40000 and 25000 yr B.P. in NW Argentina. *Palaeogeogr. Palaeoclim. Palaeoecol.*, **109**, 277–287.

Turner, J.C.M. (1970) The Andes of Northwestern Argentina. *Geol. Rundschau*, **59**, 1028–1063.

Vallance, J.W. (2000) Lahars. In: *Encyclopedia of Volcanoes* (Ed. by H. Sigurdsson, B. Houghton, S. McNutt, H. Rymer & J. Stix), pp. 601–616. Academic Press, San Diego, CA.

Vandervoort, D.S., Jordan, T.E., Zeitler, P.K. & Alonso, R. N. (1995) Chronology of internal drainage development and uplift, southern Puna plateau, Argentine central Andes. *Geology*, **23**, 145–148.

Vergés, J., Burbank, D.W. & Meigs, A. (1996) Unfolding: an inverse approach to fold kinematics. *Geology*, **24**, 175–178.

Vezzoli, L., Matteini, M., Hauser, N., Omarini, R., Mazzuoli, R. & Acocella, V. (2009) Non-explosive magma-water interaction in continental setting: examples from the Miocene magmatism of the Eastern Cordillera of Central Andes. *Bull. Volcanol.*, **71**, 509–532, doi: 10.1007/s00445-008-0239-5.

Viramonte, J., Reynolds, J.H., Del Papa, C. & Disalvo, A. (1994) The Corte Blanco garnetiferous tuff: a distinctive late Miocene marker bed in northwestern Argentina applied to magnetic polarity stratigraphy in the Río Yacones, Salta Province. *Earth Planet. Sci. Lett.*, **121**, 519–531.

Wilcox, R.E., Harding, T.P. & Seely, D.R. (1973) Basic wrench tectonics. *Am. Assoc. Petrol. Geol. Bull.*, **57**, 74–96.

Zernack, A.V., Procter, J.N. & Cronin, S.J. (2009) Sedimentary signatures of cyclic growth and destruction of stratovolcanoes: a case study from Mt. Taranaki, New Zealand. *Sed. Geol.*, **220**, 288–305.

Manuscript received 21 April 2011; In revised form 7 February 2012; Manuscript accepted 2 April 2012.